

**A Numerical Study of Equivalence in Scanning Thermistor Bolometer
Radiometers for Earth Radiation Budget Applications**

by


Martial Haeffelin

Thesis submitted to the Faculty of the
Virginia Polytechnic Institute and State University
in partial fulfillment of the requirements for the degree of
Master of Science
in
Mechanical Engineering

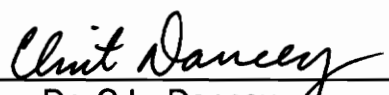
APPROVED:



Dr. J. R. Mahan, Chairman



Dr. B. Vick



Dr. C.L. Dancey

February, 1993

Blacksburg, Virginia

C.2

LO
5655
V855
1993
#1344
C.2

A Numerical Study of Equivalence in Scanning Thermistor Bolometer

Radiometers for Earth Radiation Budget Applications

by

Martial Haeffelin

J. Robert Mahan, Chairman

Mechanical Engineering

(ABSTRACT)

The Earth Radiation Budget Experiment (ERBE) consists of a suite of three scanning and four nonscanning radiometric instruments on each of three satellites which monitor the solar-reflected and Earth-emitted components of the Earth's radiative energy budget. A numerical model has been formulated to study the dynamic behavior and equivalence of the ERBE scanning thermistor bolometer radiometers.

The finite-difference method is applied to the detector of the ERBE scanning radiometer to characterize its thermal and electrical dynamic behavior. The thermal analysis confirms the thermal time constant of the instrument claimed by the vendor. The electrical model reveals that the instrument can be very sensitive to spatial variations of the incident thermal radiation. However, the analysis confirms that the hypothesis of equivalence is justified for viewing typical Earth scenes.

Acknowledgements

I would like to thank my advisor, J.R. Mahan, for his support and guidance throughout the past year and a half I have spent at Virginia Tech working on my master's degree. I am particularly thankful for the confidence he had in me, for his positive attitude in research, and for his professionalism in general. I am also grateful for the efforts he makes to offer graduate programs at Virginia Tech to half a dozen French students every year. I would also like to thank Dr. B. Vick and Dr. C.L. Dancey for serving on my advisory committee.

Thanks are extended to NASA for its graduate research assistantship support under grant NAG-1-132. Many thanks in particular to Mr. Robert B. Lee, III, and Mr. Leonard Kopia, at NASA Langley Research Center for their technical assistance.

Finally, I would like to thank my parents for the love and support they give me and for being there when I need them; to my friends without whom I would not enjoy life, thank you for being my friends.

Table of Contents

1.0 Introduction	1
1.1 The Earth and its Climate	1
1.2 Components of the Earth's Radiative Field	2
1.3 The Earth Radiation Budget Experiment (ERBE)	4
1.4 Numerical Modeling of the ERBE Radiometers	5
1.5 Motivation for this Work	6
2.0 The Scanning Thermistor Bolometer Radiometer	8
2.1 Description of the Scanning Thermistor Bolometer Radiometer	8
2.2 Optical and Radiative Analysis	10
2.3 The Detector Flake	10
3.0 Numerical Models	12
3.1 Dynamic Thermal Model of the Scanning Instrument	13
Table of Contents	iv

3.1.1	Motivation for a Numerical Model	13
3.1.2	Development of the Fully Implicit Finite-Difference Model	14
3.2	The Electrical Model	20
3.2.1	Conversion from Temperature to Resistance	20
3.2.2	Development of the Thermistor Electrical Resistance Model	21
3.3	Electronic Analysis	25
3.3.1	Description of the Detector Circuit	25
3.3.2	Analysis of the Detector Circuit	27
3.4	Integration of the Electronic Analysis and the Thermal Model . .	29
3.4.1	The Importance of Self Heating	29
3.4.2	Development of Correlations for Correction for Self Heating	30
3.4.3	Correction of Self Heating in the Thermal Model	33
3.4.4	Verification of the Correlations	33
3.4.5	Dynamic Behavior of the Electronic Circuit	34
4.0	Results and Discussion	36
4.1	The Influence of Thermophysical Properties on Dynamic Thermal Response of the Thermistor Flake	36
4.1.1	Initial Results	36

4.1.2 Results Using Realistic Thermophysical Properties . . .	39
4.2 Study of Equivalence	39
4.2.1 Point Source versus Uniform Source Distributions	40
4.2.2 Rotation of a Spatially Nonuniform Source Distribution .	41
4.2.3 Equivalence versus Nonequivalence	42
4.3 Earth Scan Simulation	43
 5.0 Conclusions and Recommendations	 45
5.1 Conclusions	45
5.2 Recommendations	46
 References	 85
 Appendix A. Computer Program Listing	 89
 Vita	 108

List of Tables

Table 1.	The Suite of Instruments Carried by Each Satellite	48
Table 2.	Thicknesses of the Layers of the Detector Flake.	49
Table 3.	Components Used in the Detector Circuit and Their Values . .	50
Table 4.	Nominal Values of the Thermophysical Properties Used in the Electrothermal Model of the Thermistor Bolometer Flake.	51

List of Illustrations		
Fig. 1	Processes Contributing to the Radiation Balance of the Earth and its Atmosphere	52
Fig. 2	Representative Spectrum of Typical Daylight Earth Scene. . . .	53
Fig. 3	The ERBE Scanning Radiometer Telescope	54
Fig. 4	Meekins' Model of the ERBE Scanning Channel.	55
Fig. 5	Thermistor Bolometer Construction	56
Fig. 6	Finite-Difference Volume Element.	57
Fig. 7	Finite-Difference Node Mesh for the Active Flake Thermal Model; (a) Plan View and (b) Front Elevation.	58
Fig. 8	Detector Bridge Amplifier Circuit	59
Fig. 9	(a) Finite-Difference Node Mesh for the Electrical Model and (b) Control Volume Element for Two-Dimensional Finite-Difference Mesh.	60
Fig. 10	Correlations Between Self Heating and Resistance in the Reference Flake.	61
List of Illustrations		viii

Fig. 11	Correlation Between Resistance of the Active Flake and Resistance of the Reference Flake.	62
Fig. 12	Numerical Results and Correlation Between Self Heating in the Reference Flake and Self Heating in the Active Flake.	63
Fig. 13	Agreement of Electronic Analysis and Thermal Model for Correlation between Self Heating and Resistance in the Reference Flake.	64
Fig. 14	Electronic Output as a Function of the Resistance of the Active Flake in Static and Dynamic Operation.	65
Fig. 15	Evolution with Time of the Temperature Profile Through the Center of the Active Flake (Thermal Conductivity of the Thermistor: 0.1 W/m-K).	66
Fig. 16	Evolution with Time of the Temperature Profile Through the Center of the Active Flake (Thermal Conductivity of the Thermistor: 1.0 W/m-K).	67
Fig. 17	Evolution with Time of the Average Thermistor Temperature.	68
Fig. 18	Evolution with Time of the Two-Dimensional Temperature Distribution in the Thermistor.	69
Fig. 19	Evolution with Time of the Temperature Profile Through the Active Flake with Self Heating and a 10-mW Radiative Power Input.	70

Fig. 20	Evolution with Time of the Average Thermistor Temperature (10-mW Radiative Power Input).	71
Fig. 21	Equilibrium Two-Dimensional Temperature Distribution in the Thermistor During a Space Look.	72
Fig. 22	Equilibrium Two-Dimensional Temperature Distribution in the Thermistor for a 10-mW Point Source Power Input.	73
Fig. 23	Equilibrium Two-Dimensional Temperature Distribution in the Thermistor for a 10-mW Uniform Source Power Input.	74
Fig. 24	Relation Between Resistance and Temperature in the Active Flake during Illumination of the Sensor by a 10-mW Uniform Source and by a 10-mW Point Source Power Input.	75
Fig. 25	Electronic Output as a Function of Time for a 10-mW Uniform Source and a 10-mW Point Source Power Input.	76
Fig. 26	Radiation Distribution on the Active Flake for Collimated Radiation Incident to the Instrument Aperture at an Angle of 1.5 deg for which 33.4 percent of energy incident to instrument aperture reaches the flake	77
Fig. 27	Equilibrium Two-Dimensional Temperature Distribution in the Active Thermistor for a 10-mW Nonuniform Source Power Input whose Shape is as in Fig. 26 but whose Size has been Increased to Fill the Absorber Surface.	78
Fig. 28	Equilibrium Two-Dimensional Temperature Distribution in the	

	Active Thermistor for the 10 mW Nonuniform Source Power Input of Fig. 27 Rotated 45 deg.	79
Fig. 29	Electronic Output as a Function of Time for the Radiative Heating Situations of Figs. 27 and 28.	80
Fig. 30	Hypothetical Earth Scene Used to Generate a Numerical Earth Scan	81
Fig. 31	Power Input to the Active Flake Corresponding to a Numerical Earth Scan Simulation Based on Fig. 30.	82
Fig. 32	Electronic Output Corresponding to the Numerical Earth Scan Simulation of Fig. 31.	83
Fig. 33	Equilibrium Electronic Output as a Function of the Power Input to the Detector for the Simulated Earth Scan of Fig. 31.	84

Nomenclature

A	Cross-sectional area (m^2)
a	Coefficient associated with nodal temperatures ($\text{W}/\text{m}^3\text{-K}$); coefficient associated with nodal potentials ($1/\Omega\text{-m}$)
C	Specific heat ($\text{J}/\text{kg-K}$)
E	Electrical potential (V)
H	Incident radiative heat flux (W/m^2)
I	Electrical current (A)
J	Electrical current density (A/m^2)
K	Coefficient related to thermophysical properties used in Eq. (1) (s/m^2)
k	Thermal conductivity ($\text{W}/\text{m-K}$)
L	Length (m)
P	Electrical power (W)
\dot{q}	Volumetric heat source (W/m^3)
q_{rad}''	Radiative heat flux (W/m^2)

R	Effective radius of the Earth (m); equivalent thermal resistance ($\text{m}^2\text{-K/W}$); electrical resistance (Ω)
S	Self heating (mW)
T	Temperature (K)
t	Time (s)
V	Volume (m^3); potential (V)
W	Width (m)
x,y	Cartesian coordinates (m)

Greek

α	Absorbivity (-), temperature coefficient ($1/\text{K}$)
β	Relaxation factor used in Eq. (16) (-)
δ	Thickness of a domain (m)
ζ	View factor from absorbing flake to field stop (-)
ξ	Factor whose value corresponds to a specific finite-difference scheme used in Eqs. (5), (6), and (7) (-)
ρ	Electrical resistivity ($\Omega\cdot\text{m}$)
σ	Stefan-Boltzmann constant ($5.6696 \times 10^{-8} \text{ W/m}^2\text{-K}$), electrical conductivity ($1/\Omega\cdot\text{m}$)

1.0 Introduction

1.1 The Earth and its Climate

The Earth is the only planet in our solar system which satisfies the necessary conditions for the development of life as we know it. Over the eons an energy equilibrium has been reached between incident solar radiation and emitted thermal radiation. A certain amount of the incident solar radiation, the *albedo*, is reflected from the Earth and its atmosphere, with the remaining being absorbed by the planet [1]. Terrestrial processes identified with the weather and climate redistribute this energy before it is ultimately re-emitted into space [2]. Perturbations such as volcanic eruptions may arise to disturb the overall equilibrium, but the solar-powered climatic engine ultimately dominates.

While the process of energy transfer into and out of the atmosphere governs the Earth's climate, human activities produce perturbations at levels which endanger

the climatic equilibrium [3]. Today the question of what will become of the Earth's climate concerns us more than ever. Will human activities such as chemical fertilization, desertification of specific areas, use of combustion engines, etc., cause inadvertent perturbations in the climate unfavorable to life on Earth? To what extent is the Earth threatened by global heating due to increased concentrations of carbon dioxide, methane, and other greenhouse gases in the atmosphere? How important is the atmospheric cloud radiative forcing? These are questions that scientists [4,5,6,7,8] are currently pondering but that are difficult to answer. The radiative energy budget of the Earth has been studied by means of satellites during the past twenty years in hopes of answering some of these questions [9,10].

1.2 Components of the Earth's Radiative Field

The radiation from a typical daylight Earth scene is composed of shortwave reflected solar radiation and longwave Earth-emitted radiation. The sun emits with a spectrum similar to that of a blackbody at a temperature of about 5780 K [11], and about 97 percent of this energy is emitted in what is called the shortwave interval between 0 and 5 μm . For our purposes, it may be assumed that scattering of solar radiation by the atmosphere and reflection from the surface of the Earth do not affect the spectral distribution. The Earth's surface receives, in addition to the flux of direct solar radiation, a flux of infrared radiation emitted by the lower layers of the atmosphere. The Earth and atmosphere reach thermal equilibrium at an average

temperature of 288 K [12]. This is a regional and seasonal average of the Earth's surface temperature T_s . The theoretical temperature of 255 K—commonly called the effective radiative temperature T_e and calculated based on the solar flux and the albedo of the planet—is the temperature at which the Earth/atmosphere system is in equilibrium with the incident solar radiation. This effective temperature is lower than T_s by 33 K [5]. The Earth/atmosphere system thus emits a spectrum similar to that of a blackbody at a temperature of about 255 K.

The solar flux incident to the top of the atmosphere is directly proportional to the luminosity of the sun and is inversely proportional to the distance squared between the sun and the Earth [5]. In order to consider only the variations intrinsic to the sun, the *solar constant* has been defined. Its value corresponds to the solar flux taking into account the average distance from the sun to the Earth, which is one astronomic unit, or 1.496×10^8 km. The solar constant is known to be $1,368 \text{ W/m}^2$ to within ± 0.3 percent [5]. The mean value of the solar flux that strikes the top of the atmosphere is the solar constant divided by four because the surface area of the Earth ($4\pi R^2$, where R is the effective radius of the Earth) is four times greater than its cross-sectional area (πR^2). This gives a value of 342 W/m^2 . The albedo of our planet has been evaluated, based on satellite data, to be about 30 percent; therefore, the reflected part of the incident energy is close to 102 W/m^2 [1,5].

The mean thermal infrared flux emitted by the Earth/atmosphere system has been evaluated to be about 240 W/m^2 [1,5], which gives a net radiative balance of zero when averaged over time and at the top of the Earth's atmosphere. The

processes contributing to the radiation balance of the Earth are shown in Figure 1.

In an average daylight Earth scene 30 percent of the energy monitored by a radiometer on board a satellite and looking down at the Earth will be concentrated in the shortwave (solar) part of the spectrum and 70 percent will be concentrated at the long (Earth-emitted) wavelengths. In order to take into account both spectral distributions, an equivalent spectrum is computed by weighting each spectrum with its respective contribution to the total Earth radiation field. The resulting spectrum is shown in Figure 2.

1.3 The Earth Radiation Budget Experiment (ERBE)

The Earth Radiation Budget Experiment (ERBE) was started by the National Aeronautics and Space Administration (NASA) in the early 1980's to monitor the thermal radiation field of the Earth. This program aims at understanding weather evolution over long periods of time and over defined geographical regions.

ERBE became operational after two satellites, NASA's Earth Radiation Budget Satellite ERBS and the National Oceanic and Atmospheric Administration's NOAA-9, were launched in 1984. In 1986 a third set of instruments was launched on board NOAA-10 [13]. Each satellite carries the suite of radiometers described in Table 1. The scanning radiometers on board each satellite, on which the work presented in this thesis is based, are narrow field-of-view instruments. There are three scanning instruments per satellite in order to cover the three wavelength

intervals: a shortwave visible channel, a longwave channel, and a total channel [14].

The scanning radiometers, which consist of a thin-film thermistor bolometer viewing the Earth through a Cassegrain telescope, are described in Section 2.0. The nonscanning instruments mentioned in Table 1 are active cavity radiometers. Description of the nonscanning instruments may be found elsewhere [20,22].

1.4 Numerical Modeling of the ERBE Radiometers

Graduate students under the supervision of Professor J.R. Mahan have worked on projects concerning the Earth radiation budget since the beginning of the 1970's. From theoretical studies of the radiative characteristics of spherical cavities by Fanney [15], Rasnic [16], and Passwaters [17], the work of the *Radiation Science Group* at Virginia Tech has evolved to encompass applied numerical modelling projects. Eskin [18] was the first to use a Monte-Carlo-based ray-trace technique to model active cavity radiometers. Gardiner [19] studied the operation of ERBE-type active cavity radiometers at cryogenic temperatures. Most recently, the aim of the *Radiation Science Group* is to develop end-to-end models of the ERBE scanning and nonscanning radiometers and the CERES scanning radiometers. These numerical representations usually consist of a Monte-Carlo-based ray-trace, a finite-difference- or finite-element-based diffusion model, and an analysis of the electronics involved in the instrument. The ray-trace numerical representation is generally a spectral model of the radiation heat transfer involved in the functioning

of the radiometer. It characterizes the specific geometry of the device and the influence that each element has on its response. The diffusion model characterizes the dynamic behavior of the active part of the instrument, and links the radiative input to the electronic response of the radiometer. Finally, the dynamic analysis of the detector electronic circuit concludes the characterization of the transfer function, defined as the ratio of the electronic signal output of the instrument to the radiative power input. The development achieved so far includes the work of Eskin [18], Gardiner [19], Tira [20,22,23,24,25], Meekins [21,24,25], and this author.

1.5 Motivation for this Work

This thesis presents the effort involved in the development of a three-dimensional transient diffusion model of the active flake of a scanning bolometer radiometer, the dynamic electronic analysis of its detector circuit, and the integration of these models with each other and with a pre-existing optical model [21]. The diffusion model subdivides the active flake into a sufficiently large number of volume and surface elements to sample all of the parameters to which the instrument response may be sensitive. It is formulated at a level which permits assessment of the influence of changes in the temperature or thermophysical properties of one element on the temperature of any other element. The electronic analysis accounts for the thermal and electrical dynamic behavior of each device used in the detector circuit. This level of analysis is necessary for an accurate correlation with the

thermal effects characterized in the dynamic thermal model.

The combination of the two models permits the issue of self heating of the detector of the scanning instrument to be addressed. In addition, the combined model can be used to reveal the degree to which the spatial distribution of the input signal on the sensor influences the response of the instrument. This latter is the so-called *equivalence* issue.

These models, combined with a numerical characterization of the optical part of the instrument [21] and a diffusion analysis of the body of the instrument, currently being done by another graduate student, form an end-to-end channel model. Each part of the end-to-end model is developed to achieve a tool which permits the user to evaluate the sensitivity of the instrument response to design parameters such as dimensions, material properties, manufacturing methods, and the nature of the source field being viewed.

2.0 The Scanning Thermistor Bolometer Radiometer

2.1 Description of the Scanning Thermistor Bolometer Radiometer

The scanning instruments carried by each ERBE and CERES satellite consist of Cassegrain telescopes viewing the same Earth scene in different parts of the spectrum of the Earth's radiative field. As developed in Section 1.2, it is important to make a distinction between different categories of radiation with respect to wavelength. With the use of filters, for a given Earth scene the longwave and shortwave radiation can be separated without significant loss or "double accounting" of information, as suggested by the representative Earth radiation field spectrum of Figure 2. The shortwave channel is equipped with a Suprasil-W2 silica glass filter which has a high transmissivity for radiation in the wavelength interval 0.2 to 5.0

μm . A diamond filter which transmits radiation in the interval 5.0 to 50.0 μm is used for the longwave channel. The third channel is an unfiltered "total" channel which has a passband of 0.2 to 100.0 μm . The spectral characteristics of these filters are given by Meekins [21].

The optical system of each telescope is based on a design developed in 1672 by the French scientist, N. Cassegrain. It uses two aspherical mirrors, a primary concave paraboloid, and a secondary convex hyperboloid, as shown in Figures 3 and 4. The mirrors are coated with aluminized schott glass for protection against ultraviolet radiation which could cause degradation and alteration of their optical properties. The spectral response of the mirrors is also given in reference 21.

Radiation enters the instrument through the baffle. The design of the baffle, the reflector cap, and the detector housing maximizes attenuation of off-axis radiation as explained by Meekins [21]. The surfaces of the reflector cap facing the opening of the baffle are highly reflective, to reflect out off-axis radiation, whereas those facing the interior of the instrument are highly absorptive, to capture radiation reflected from interior surfaces of the telescope. Finally, the V-groove of the detector housing is also very absorptive; radiation entering it has a very low probability of escaping. For a diffuse source, only a very small fraction of the radiation incident to the baffle actually strikes the active flake [21]. Rays nearly parallel to the instrument optical axis are specularly reflected on the primary and secondary mirrors successively before entering the field stop behind the primary mirror. The absorber flake is mounted behind the field stop on a large aluminum

block which serves as a heat sink.

2.2 Optical and Radiative Analysis

Optical and thermal numerical models of the ERBE scanning channels have already been formulated by Meekins [21], who applied the Monte-Carlo ray-trace method to spectrally characterize the optical performance (optical transfer function) and the thermal radiative performance (thermal noise). The optical analysis showed that the radiometer effectively limits the amount of energy which reaches the active sensor, as expected. It was found that radiation further off axis than about 3.0 deg does not reach the active flake, and thus is rejected. The radiative analysis showed thermal emission from the scanning radiometer assembly to the active flake can attain up to 2.2 percent of the incoming signal [21]. However, Meekins' model does not account for the instrument dynamic behavior associated with thermal diffusion and the electronic circuit, nor does it evaluate instrument equivalence.

2.3 The Detector Flake

The active element of the scanning radiometer, also referred to as the detector, consists of a thermistor bolometer in a bridge circuit. The bolometer is a composite flake made up of extremely thin layers of specific materials, as shown in

Figure 5. The reader should note that Figure 5 shows the detector flake developed for CERES, which is an improved version of the detector used in ERBE. The main improvements are related to the assembly of the different layers and the quality of electrical insulation of the conducting layer.

The layer receiving incident radiation is a flake made of black Chemglaze Z-306 paint with 10 percent additional carbon to augment its absorbance. The incident energy absorbed by the absorber flake is conducted three-dimensionally within the bolometer. As will be seen later, heat is conducted in a principal direction. The absorber flake is sealed and bonded to the thermistor flake by a layer of epoxy. The thermistor is a semiconducting material consisting of a polycrystalline metal with a Cobalt-Nickel-Manganese oxide spine whose electrical resistance is highly temperature sensitive [26]. It is linked to the external circuit by platinum detector leads welded to two thin gold contact pads. The thermistor layer communicates thermally with the aluminum-alloy heat sink through a thin film of Kapton which acts as a thermal impedance. The thermal impedance is important since it allows the flake to heat up when radiation falls on it; without the thermal impedance the flake would stay at the temperature of the heat sink [27]. The detector flake, which has a 3.0 mm by 1.5 mm rectangular shape, is about 44 μm thick; the detailed dimensions of each layer are given in Table 2.

Conduction heat transfer in the active flake is modeled using a fully implicit finite-difference method as described in Chapter 3.

3.0 Numerical Models

The finite-difference-based models of the thermal and electrical dynamic behavior of the detector are developed in this chapter. The thermal model characterizes the temperature changes in the detector flake associated with temporal and spatial variations of the radiative input. The electrical model predicts the variation of overall resistance of the flake due to thermal changes. The model, which we have named *DYNASCAN*, has been programmed in FORTRAN. In addition, an electronic analysis has been performed to model the dynamic behavior of the electrical circuit, and the thermal, electrical, and electronic models have been integrated.

3.1 Dynamic Thermal Model of the Scanning Instrument

3.1.1 Motivation for a Numerical Model

A numerical approach has been chosen because the heat conduction problem is three-dimensional, unsteady and has a nonlinear radiative boundary condition. Exact analytical methods are in this case very difficult if not impossible to apply [28]. The finite-difference method is conceptually simple and straightforward, and it is suitable for rectangular geometries. Another advantage of this method is that the physical problem appears clearly in the finite-difference discretized problem statement. The fully implicit scheme is not the most accurate or easiest scheme, but it is unconditionally stable, whereas the more accurate Crank-Nicolson and the easier explicit schemes impose the stability criterion

$$\Delta t \leq K \Delta x^2 \quad , \quad (1)$$

on the calculation time step. In Equation 1, K is a coefficient related to the thermophysical properties of the material and Δx is the grid spacing. Since one of the dimensions of the problem is on the order of a few micrometers, the stability criterion would require prohibitively small time steps to achieve a stable solution.

3.1.2 Development of the Fully Implicit Finite-Difference Model

Since the thermophysical properties of the materials vary from one layer to the next, the finite-difference model is initially developed from the point of view of control volumes. Each layer is first subdivided into control volumes such that the properties are constant within a given control volume. The nodes are located at the centers of the control volumes. Each node has six neighbors: **North**, **South**, **West**, **East**, **Front**, and **Back**, as shown in Figure 6. In a finite-difference model the temperature of a node **P** is directly related to the temperatures of its six neighbors. In addition, because the problem is unsteady, the temperature of node **P** at time t also depends on its temperature at the previous time step, $t-\Delta t$.

The active flake, shown in Figure 7, is geometrically three-dimensional. Although we know that heat is conducted principally in one direction, the three-dimensionality of the problem is retained in order to maintain the flexibility of the model and to sample the effects of three-dimensionality. The unsteady heat conduction equation may be written

$$\frac{\partial}{\partial x}\left(k_x \frac{\partial T}{\partial x}\right) + \frac{\partial}{\partial y}\left(k_y \frac{\partial T}{\partial y}\right) + \frac{\partial}{\partial z}\left(k_z \frac{\partial T}{\partial z}\right) + \dot{q} = \rho C \frac{\partial T}{\partial t} , \quad (2)$$

where k_x , k_y and k_z are the thermal conductivities in the x , y and z directions, respectively, ρ is the mass density, C is the specific heat, and \dot{q} is the internal heat generation term. The notation used is that of Patankar [28]. In this notation, upper-

case subscripts indicate nodal values whereas lower case subscripts represent control-volume-face values.

The discretized equation is then obtained by integrating Equation 2 over time and over the control volume shown in Figure 6, yielding

$$\begin{aligned} & \int_{cv} \int_t^{t+\Delta t} \frac{\partial}{\partial x} \left(k_x \frac{\partial T}{\partial x} \right) dt dV + \int_{cv} \int_t^{t+\Delta t} \frac{\partial}{\partial y} \left(k_y \frac{\partial T}{\partial y} \right) dt dV \\ & + \int_{cv} \int_t^{t+\Delta t} \frac{\partial}{\partial z} \left(k_z \frac{\partial T}{\partial z} \right) dt dV + \int_{cv} \int_t^{t+\Delta t} \dot{q} dt dV = \int_{cv} \int_t^{t+\Delta t} \rho C \frac{\partial T}{\partial t} dt dV . \end{aligned} \quad (3)$$

The temperature T_p at node **P** is assumed to prevail over the entire control volume. Then using T_p for the temperature at time step t and T_p^0 for the temperature at the previous time step $t-\Delta t$, the right-hand side of Equation 3 can be approximated

$$\int_{cv} \int_t^{t+\Delta t} \rho C \frac{\partial T}{\partial t} dt dV = \rho C (T_p - T_p^0) \Delta x \Delta y \Delta z . \quad (4)$$

If we proceed to the integration of the first term on the left-hand side of Equation 3 there results

$$\begin{aligned} \int_{cv} \int_t^{t+\Delta t} \frac{\partial}{\partial x} \left(k_x \frac{\partial T}{\partial x} \right) dt dV = & \left(\frac{1}{R_w} [\xi T_w + (1 - \xi) T_w^0] + \frac{1}{R_\theta} [\xi T_\theta + (1 - \xi) T_\theta^0] \right. \\ & \left. - \left(\frac{1}{R_w} + \frac{1}{R_\theta} \right) [\xi T_p + (1 - \xi) T_p^0] \right) \Delta y \Delta z \Delta t , \end{aligned} \quad (5)$$

where ξ is a factor whose value corresponds to the scheme chosen: $\xi=0$ for fully explicit, $\xi=0.5$ for Crank-Nicolson, and $\xi=1$ for fully implicit. In Equation 5 R_e is the equivalent resistance between node **P** and its neighbor **E**. It includes the resistance of the material in the control volume of node **P**, the resistance of the material in the control volume of node **E**, and the contact resistance between the two control volumes. Similarly R_w is the equivalent resistance between nodes **P** and **W**. The other two diffusion terms on the left-hand side of Equation 3 are integrated in a similar fashion, yielding

$$\int_{cv} \int_t^{t+dt} \frac{\partial}{\partial y} \left(k_y \frac{\partial T}{\partial y} \right) dt dV = \left(\frac{1}{R_f} [\xi T_f + (1 - \xi) T_f^0] + \frac{1}{R_b} [\xi T_b + (1 - \xi) T_b^0] \right. \\ \left. - \left(\frac{1}{R_f} + \frac{1}{R_b} \right) [\xi T_p + (1 - \xi) T_p^0] \right) \Delta x \Delta z \Delta t, \quad (6)$$

and

$$\int_{cv} \int_t^{t+dt} \frac{\partial}{\partial z} \left(k_z \frac{\partial T}{\partial z} \right) dt dV = \left(\frac{1}{R_n} [\xi T_n + (1 - \xi) T_n^0] + \frac{1}{R_s} [\xi T_s + (1 - \xi) T_s^0] \right. \\ \left. - \left(\frac{1}{R_n} + \frac{1}{R_s} \right) [\xi T_p + (1 - \xi) T_p^0] \right) \Delta x \Delta y \Delta t. \quad (7)$$

Finally, integration of the volumetric source term yields,

$$\int_{cv} \int_t^{t+dt} \dot{q} dt dV = \dot{q} \Delta x \Delta y \Delta z \Delta t. \quad (8)$$

Setting ξ equal to unity, dividing Equations 4, 5, 6, 7, and 8 by $\Delta x \Delta y \Delta z \Delta t$, and

moving T_p to the left-hand side and the other temperatures to the right-hand side yields

$$a_p T_p = a_p^0 T_p^0 + \sum_n a_n T_n + \dot{q} \quad , \quad (9)$$

where

$$a_p^0 = \frac{\rho C}{\Delta t} \quad , \quad (10)$$

$$a_n = \frac{1}{\Delta x_n R_n} \quad , \quad (11)$$

and

$$a_p = a_p^0 + \sum_n a_n \quad . \quad (12)$$

The subscript "n" in Equations 9 through 12 refers to "neighbor".

The boundary conditions may be stated as follows. As a matter of convenience the edges of the active flake are considered to be insulated. The true edge condition is a radiative boundary condition, but the edges are extremely thin and their temperature is very close to that of the surroundings; therefore, they may be considered insulated for all practical purposes. The top surface of the absorber flake receives radiation from the scene through the telescope, and also exchanges heat with its surroundings by radiation. The radiative environment of the active flake can best be appreciated by reference to Figure 4. The net radiative heat flux distribution on the top boundary is considered to be known. Finally, at the bottom the lower bonding layer of the thermal impedance is considered to be in thermal

contact with a known constant-temperature heat sink, and so the boundary condition used here is a given temperature value.

The net radiative heat flux incident to the absorber flake is

$$q''_{rad} = q''_{rad\ in} - q''_{rad\ out} \quad . \quad (13)$$

The incoming radiation, $q''_{rad\ in}$, is composed of an incident radiative flux H , which arrives through the telescope from the source field, and energy absorbed from the flake surroundings at an equivalent radiation temperature T_{sur} . The radiation out, $q''_{rad\ out}$, is emitted by the absorber flake due to its temperature T_p . In terms of temperatures Equation 13 may be written

$$q''_{rad} = \alpha[\zeta H + (1 - \zeta)\sigma(T_{sur})^4 - \sigma(T_p)^4] \quad , \quad (14)$$

where α is the absorptivity of the flake, ζ corresponds to the view factor from the absorbing flake to the field stop, and σ is the Stefan-Boltzmann constant. Equation 14 introduces a nonlinear term to the problem. The nonlinearity can be removed by linearization of the fourth-order T_p term but it then becomes necessary to iterate to obtain the solution. Linearization of Equation 14 yields

$$q''_{rad} = \alpha[\zeta H + (1 - \zeta)\sigma(T_{sur})^4] - 3\alpha\sigma(T_p^*)^4 + 4\alpha\sigma(T_p^*)^3 T_p \quad , \quad (15)$$

where T_p^* is the temperature T_p at the previous iteration. This linearization represents the tangent to the q''_{rad} versus T_p curve at T_p^* .

The algorithm of the finite-difference code, which uses a Gauss-Siedel point-

by-point method to solve the algebraic equations of the problem, is developed in reference 28. In the current implementation it starts with an initial temperature, usually 311 K, for the entire grid. An initial temperature guess is assigned to each node in order to calculate the node temperatures at the first time step. Each grid point, or node, is visited successively to calculate the temperature at this point, using the discretized Equation 9. The temperatures of the six neighbors are simply the latest values available. When the entire grid has been visited in this manner one iteration is completed. Iterations are performed successively until the change in node temperatures from one iteration to the next becomes less than a given value.

To change the speed of convergence, that is, to change the number of iterations necessary to obtain a converged solution, a convergence term can be added to the discretized Equation 9. Equation 9 then takes the form

$$T_p = \beta \frac{\left(a_p^0 T_p^0 + \sum_i a_i T_i + \dot{q} \right)}{a_p} + (1 - \beta) T_p^* , \quad (16)$$

where β is a relaxation factor. For strongly nonlinear equations the iterative solution might tend to diverge, in which case the changes in the values of T_p over one iteration must be reduced. In this case an underrelaxation factor can be used; that is, β is given a value between 0 and 1. If the solution is well behaved, the changes

of T_p from one iteration to the next can be speeded up by using an overrelaxation factor; that is, β is given a value greater than unity.

When the node temperatures have converged for one time step they are stored and another iterative process can start for the following time step. The initial temperatures for the new time step are then the converged values of the previous one. The time is increased until the change in node temperatures from one time step to the next becomes less than a given value. The temperature distribution in the active flake is then said to have reached steady state.

3.2 The Electrical Model

3.2.1 Conversion from Temperature to Resistance

The active and reference flakes are mounted in a detector bridge circuit as shown in Figure 8. In each flake, the current passes through the thermistor layer connected to the circuit by the platinum leads. The resistance provided by a square sheet of thermistor is directly related to its temperature. For small variations of temperature this relation can be approximated by

$$R = R_0[1 - \alpha(T - T_0)] \quad , \quad (17)$$

where R_0 is a known thermistor resistance at temperature T_0 and α is the temperature coefficient of resistance around T_0 [26].

When the active flake receives a radiative heat input, its temperature distribution changes rapidly which in its turn changes the overall resistance of the thermistor. Equation 17 cannot be used to relate the average temperature of the thermistor to its overall resistance. Instead, given an assumed electrical potential difference across the flake, a discrete electric field is computed using the two-dimensional electric diffusion equations. Local electrical conductivity is computed from local temperatures given by the thermal model. The current density passing through the flake is then computed by applying Ohm's law locally. Finally, the overall resistance of the thermistor is computed as an equivalent resistance; that is, as the ratio of the applied potential difference to the computed total current. This procedure is described in detail in the following section.

3.2.2 Development of the Thermistor Electrical Resistance Model

In order to accurately compute the overall resistance of the flake, the electric field in the thermistor corresponding to a given bias potential difference applied between the two gold pads must first be determined. The steady electric field is represented on a two-dimensional mesh where the control-volume faces lie midway between the nodes, as shown in Figure 9(a). The principle of conservation of electrical charge applied over the control volume shown in Figure 9(b) leads to the relation

$$\frac{\partial J_x}{\partial x} + \frac{\partial J_y}{\partial y} = 0 , \quad (18)$$

where J_x and J_y are current densities in the x and y directions, respectively. Ohm's law yields

$$J_x = -\sigma \frac{\partial E}{\partial x} \quad (19)$$

and

$$J_y = -\sigma \frac{\partial E}{\partial y} \quad (20)$$

where E represents the electrical potential and σ is the electrical conductivity.

Substituting Equations 19 and 20 into Equation 18 yields the Laplace equation,

$$\frac{\partial}{\partial x} \left(\sigma \frac{\partial E}{\partial x} \right) + \frac{\partial}{\partial y} \left(\sigma \frac{\partial E}{\partial y} \right) = 0 . \quad (21)$$

The discretized formulation of Equation 21 is obtained by the control volume method already developed in Section 3.1.2. Using notation from Figure 9(b), Equation 21 becomes

$$a_P E_P = a_E E_E + a_W E_W + a_N E_N + a_S E_S , \quad (22)$$

where

$$a_E = \frac{\sigma_e \Delta y}{\delta x_e} , \quad a_W = \frac{\sigma_w \Delta y}{\delta x_w} , \quad (23)$$

$$a_N = \frac{\sigma_n \Delta x}{\delta y_n} , \quad a_S = \frac{\sigma_s \Delta x}{\delta y_s} , \quad (24)$$

and

$$a_P = a_E + a_W + a_N + a_S . \quad (25)$$

Given a discrete temperature distribution from a two-dimensional mesh, as shown in Figure 9(a), electrical conductivities σ are calculated for each control volume assuming that the nodal temperature prevails over the entire control volume. Electrical resistivity ρ is related to electrical resistance R by

$$\rho = R \frac{W\delta}{L} , \quad (26)$$

where L is the length, W is the width, and δ is the thickness of the domain. Therefore, σ is related to the temperature by

$$\sigma = \frac{L}{W\delta} \frac{1}{R_o [1 - \alpha(T - T_o)]} . \quad (27)$$

The values of electrical conductivity used in Equations 23 and 24 are control-volume-face values; they are computed using a harmonic mean formulation which

yields, at face e for example,

$$\sigma_e = \frac{2\sigma_E\sigma_P}{\sigma_E + \sigma_P} . \quad (28)$$

In Equation 28 upper-case subscripts indicate nodal values whereas lower-case subscripts represent control-volume-face values. The harmonic mean is more accurate than the arithmetic mean, especially when the difference between σ_E and σ_P is large.

The boundary conditions are of two kinds: insulated boundaries along the length of the flake and applied electrical potentials at each end of the flake.

Computation of the discrete distribution of electrical potential involves solving a set of linear equations of the type of Equation 22. For two-dimensional problems, direct solving methods involve pentdiagonal matrices and are therefore very computer intensive with respect to storage and memory. Iterative methods are easy to use and usually more computer efficient. Similarly to the thermal model, a Gauss-Siedel point-by-point overrelaxed method is used to obtain the discretized solution. The algorithm is similar to that described in Section 3.1.2 for a single time step.

When the electric field is computed, the current density passing across the thermistor flake is integrated over the cross-section at each end of the flake to obtain the current. Kirchoff's current law

$$I_{in} - I_{out} = 0, \quad (29)$$

is then checked, where I_{in} is the current entering the thermistor at one boundary and I_{out} is that leaving at the other boundary. The current at either boundary is obtained by using the discretized version of Equation 19, in which E is represented by a piece-wise linear profile,

$$I = \sigma \left(\frac{E_i - E_{i-1}}{\Delta x} \right) A , \quad (30)$$

where A is the cross-sectional area of the thermistor flake. There exists an equivalent resistance R , across which a given bias potential difference ΔV_o would produce the current I . Then according to Ohm's Law

$$R = \frac{\Delta V_o}{I} , \quad (31)$$

where R is the equivalent resistance of the thermistor flake.

3.3 Electronic Analysis

3.3.1 Description of the Detector Circuit

The detector circuit shown in Figure 8 transforms variations of the thermistor resistance into fluctuations of the electrical output signal. Figure 8 is based on

references 29 and 30. As already mentioned, the active and reference flakes are mounted in an electrical bridge circuit along with two other fixed resistors. When the radiative power incident to the active detector is zero, the bridge is in balance and no output voltage is produced. The idea behind the detector bridge is that if the heat sink temperature changes, the effective temperature and resistance of the reference and active flakes will change by the same amount. Therefore the balance (or unbalance) of the bridge will remain unchanged and so will the output signal.

Since the reference flake does not receive any of the radiative heat input, its temperature should remain constant at the heat sink temperature and thus the resistance in one arm of the bridge should remain constant. When the active flake receives a radiative heat input, the resistance of the thermistor changes rapidly, and the bridge becomes unbalanced, thereby producing an output signal. Also, the level of self heating changes in both thermistors with changes in radiative input to the active thermistor, as described in Section 3.4.

The other elements of the circuit shown in Figure 8 are the ballast resistors, R_a and R_b , the bridge fixed resistors R_3 and R_4 , the low-pass filter composed of R_5 and C_1 , and the operational amplifier and its feedback loop composed of R_7 and C_2 . The ballast resistors are used to adjust the electric potential difference applied to the bridge. The bridge fixed resistors R_3 and R_4 each consist of a large fixed resistor in series with a smaller resistor whose resistance can be varied. These smaller resistors are used to establish the prelaunch bridge balance condition for zero radiative input. The low-pass filter limits the frequency content of the time

varying signal that goes to the operational amplifier. The feedback loop converts the operational amplifier into an integrating amplifier. The characteristics of the electrical components are summarized in Table 3.

The circuit output signal V_s produced by the scanning radiometer is encoded for transmission to Earth. It is therefore important to accurately relate the resistance of the thermistor to the output signal.

3.3.2 Analysis of the Detector Circuit

A commercial software package, PSpice® [32], developed by the MicroSim Corporation, does electronic circuit analysis and is available for free! The devices of the circuit, such as the power supplies, the resistors, the capacitors, and any active component such as operational amplifiers must be carefully defined in the input file to PSpice®. Parameters such as the temperature of the circuit environment can even be specified to enhance the accuracy of the model. An analysis sequence is defined as a sweep over a range of values of a source, where the source usually is an independent potential difference or current. Unfortunately no predefined analysis command exists to model a time-varying resistor such as the thermistor; therefore PSpice® must be "tricked" into performing the analysis required for the current problem [31].

A *voltage-controlled voltage source* device, E1, is defined between an artificial node and a zero-voltage node. The controlling input is TIME. Normally the

output value of E1 for each given input time would be a potential difference, that of the artificial node. Instead, the output value associated with each input time is chosen to be a discrete value of the resistance of the thermistor obtained from the thermistor electrical resistance model described in Section 3.2.2. Furthermore, a *voltage-controlled current source* device, G1, is defined at the location of the active thermistor, between nodes 1 and 3 in Figure 8. The input value must either be a potential difference or a ratio of potential differences, and is thus chosen to be the ratio of the potential difference across G1 and the potential difference of the artificial node. Since the latter potential difference is in fact a value of the thermistor resistance, the output value for this device controls the current passing through G1. For each time value input to E1, the current through the thermistor G1 is controlled by the resistance of the thermistor at that time.

The procedure in PSpice® for a dynamic analysis is called *TRAN*, for transient. The transient analysis starts at time zero, and marches forward to a specified final time using at least fifty time steps. To obtain the results of the transient analysis, the use of the printing command is necessary. Values of interest are, for example, the potential difference across and current through both thermistor flakes, as well as the output signal of the circuit.

Certain circuit parameters can be adjusted to optimize the behavior of the detector circuit, but most parameters are as in reference 30. The power supply for the operational amplifier, represented by V_s in Figure 8, is set to 22 V because of the range of the radiative power input. The feedback resistance R_7 used in the

current analysis is lower than the value communicated in reference 30. The compensating resistances in the bridge are adjusted to obtain an output signal as close to zero as possible when the sensor views space.

This complex analysis allows an experimental relation between the resistance of the active thermistor and the circuit signal response to be established. In addition, the electrical power dissipated in the thermistor layer of each flake is easily computed as the product of the potential difference across them and the current passing through them. Several effects can then be studied:

1. The importance of self heating in either flake, and its influence on the response,
2. The difference between self heating in the active and reference flakes,
3. The influence of time delay of the circuit on the response of the instrument.

3.4 Integration of the Electronic Analysis and the Thermal Model

3.4.1 The Importance of Self Heating

Self heating occurs in the thermistor layers of the active and reference flakes when electric current passes through them. The power generated P is related to the resistance R and the current I , or the potential difference ΔV and the current I , by

$$P = I^2 R = I \Delta V. \quad (32)$$

It was found in the electronic analysis that self heating of the thermistors is not negligible when compared to the radiative power input. Self heating is actually on the order of 50 mW, which is five times greater than the radiative power input used in the various numerical experiments. Since self heating is important it has to be considered in the thermal analysis.

The ideal analysis would require the electrothermal and electronic models to be linked such that feedback from one model to the other occurs at each iteration, or more reasonably at each time step. Unfortunately, the electrothermal model is formulated in FORTRAN and the commercial software PSpice® requires a very specific format for the input file which is incompatible with FORTRAN. In addition, transient analysis in the PSpice® electronic model can only be started at time zero. Total linkage implies that the FORTRAN code *Dynascan*, which performs the dynamic electrothermal analysis, should include the electronic analysis such that self heating could be updated at each time step. Therefore, direct linkage has not been implemented. Instead, a careful study of the results of the electronic analysis has allowed development of an indirect linkage procedure based on certain correlations.

3.4.2 Development of Correlations for Correction for Self Heating

In the initial thermal model, self heating was assumed to be constant. Since self heating was considered constant in the reference flake, the resistance of the

thermistor in that flake was also constant because there is no other power input. The changes of the resistance of the active flake were then assumed to be solely due to the radiative power input. Results of the electronic analysis show that under these conditions, the product of the current through and the potential difference across the resistors, which represents self heating, increases during a transient analysis. The maximum changes due to self heating in the reference and active flake resistances has been evaluated to be 1 mW and 0.2 mW, respectively, or 2 percent and 0.4 percent increases, respectively.

A correlation between self heating and resistance of the reference flake is derived from data computed using the dynamic thermal model. The resistance of the reference flake is calculated for different values of self heating using the dynamic thermal model with zero radiative power input and with zero heat loss through the telescope; that is, assuming it sees only a surroundings at 311.15 K. The correlation is represented by the linear regression model

$$R_r = - 0.353S_r + 136.25, \quad (33)$$

where R_r is the resistance in the reference flake in $k\Omega$ and S_r is the self heating in the flake in mW. The "R-squared" value associated with the correlation, which represents the proportion of variability explained by the regression model, is 0.9997. Additional linear correlations between self heating and resistance in the reference flake are derived from data computed in the dynamic electronic analyses. Each

correlation is obtained for a given value of the resistance in the active flake. These correlations along with Equation 33 are represented in Figure 10.

It is clear from the physics that the thermal and electronic analyses must agree; the system can operate only for values which satisfy both models. A relationship between the resistance in the active flake R_a and the resistance in the reference flake R_r is derived from the operating values circled in Figure 10. This correlation, shown in Figure 11, has the form

$$R_r = 0.14R_a + 101, \quad (34)$$

where the resistances are in $k\Omega$. The "R-squared" value for this linear regression is 1.0000.

Finally, a correlation between self heating in the two flakes can be obtained from output data of the electronic analysis. The correlation is again linear and the corresponding regression is

$$S_r = 0.222S_a + 41.45, \quad (35)$$

where S_r and S_a are self heating in the reference flake and active flake, respectively, in mW. The "R-squared" value is 0.9950. Numerical results and Equation 35 are compared in Figure 12.

3.4.3 Correction of Self Heating in the Thermal Model

Self heating is known to vary as the resistance changes in both flakes and with time. In the thermal model, the resistance of the active flake R_a is computed from the temperature distribution in the thermistor at each time step. Self heating in the active flake S_a corresponding to R_a can be found by eliminating R_r and S_r among Equations 33, 34, and 35. The resulting correlation is

$$S_a = -0.088R_a + 63.619. \quad (36)$$

The accuracy of this correlation depends on the number of significant figures carried. The thermal model uses double-precision.

3.4.4 Verification of the Correlations

Equation 33 is a correlation obtained from numerical results using the thermal analysis. Figure 13 shows three sets of data obtained from the electronic analysis which verify the correlation derived from the thermal model. The three sets correspond to three numerical experiments with different radiative power inputs. The agreement between the thermal-model-based correlation and the electronic-analysis data is satisfactory.

Equation 35 was derived from a set of numerical data obtained in the

electronic analysis. Figure 12 shows the set of data used to derive Equation 35 (data set 1) and the correlation. Numerical data sets 2 and 3, also shown in Figure 12, have been computed after modification of the thermal model. This illustrates the good consistency of the correlations presented in Section 3.4.2.

3.4.5 Dynamic Behavior of the Electronic Circuit

For a given constant heat input on the detector, the dynamic thermal model generates a table containing discrete values of the overall resistance of the active thermistor. At time equal to zero the value of the overall resistance of the thermistor is that corresponding to steady-state with zero radiative power input. In fact, heat is leaving the flake since the detector can "see" space, which is a body at essentially 0 K, through the telescope optics. For time greater than zero, with a constant net power input, the resistance in the thermistor decreases and the discrete resistance value is updated every millisecond. The resistance of the reference flake is computed from the resistance of the active flake using Equation 34, as developed in Section 3.4.2.

The values of the resistance of the active and reference thermistors are used as an input to the dynamic electronic analysis, such that the output voltage of the detector circuit becomes a function of the resistances which are themselves a function of time. Program PSpice[®] computes a table of output signals.

The time delays related to the electronics can be appreciated by comparing

the dynamic analysis to a static analysis. The static analysis is performed by computing the steady-state signal responses (in volts) corresponding to a sequence of thermistor resistance values. The dynamic and static analysis are compared in Figure 14.

4.0 Results and Discussion

Presented in this Chapter are the influence of thermophysical properties on the dynamic response of the detector flake, the importance of the issue of equivalence, and the results from a simulated Earth scan.

4.1 The Influence of Thermophysical Properties on Dynamic Thermal Response of the Thermistor Flake

4.1.1 Initial Results

When the model was first tested nominal values of thermophysical properties were not known for some materials. The thermal conductivity of the Kapton impedance was basically the only property available from the vendor. The

properties of gold and epoxy were found in the literature whereas those of the absorber and thermistor flakes had to be guessed. Under these conditions the thermal conductivities of the absorber and the thermistor must be treated as parameters; therefore, the results obtained are to be associated with one set of parameter values. Other parameters are of course the amount of radiation incident to the flake, as well as the spatial distribution of that radiation.

For preliminary studies the energy incident to the radiometer was chosen to be that corresponding to a typical daylight Earth scene as described in Section 1.2. Self heating was ignored in these preliminary studies.

In order to accurately model the dynamic thermal response of the active flake to a given incident flux, a "space-look" simulation is performed prior to the experiment; that is, the model is run with the radiative input (H in Equation 14) set to zero. The equilibrium temperature of the flake is reached after about 50 ms. The temperature profile obtained, the bottom profile in Figure 15, serves as the initial temperature distribution for the Earth observation simulation experiment. A given incident flux is then applied and the transient three-dimensional temperature calculation is performed. Figures 15 and 16 show the temperature profile through the center of the active flake at a series of time steps for two different assumed values of the thermistor material thermal conductivity. Steady state is reached in less than 50 ms. The results of Figure 15 have been obtained with a thermal conductivity for the thermistor of 0.1 W/m-K, which is on the order of the thermal conductivities of the other materials. This explains why the slope of the profile

remains fairly constant throughout the flake. Figure 16 clearly shows a plateau where there is almost no temperature gradient, which is characteristic of a higher thermal conductivity, 1.0 W/m-K, of the thermistor material.

The average thermistor temperature based on two x-y planes of 48 nodes each varies with time as shown in Figure 17. The time constant of a system is the time necessary for the response to reach 62 percent of its steady-state value for a step-function input. The time constant has been evaluated graphically for the thermistor in Figure 17; the value of about 10 ms is close to the performance of 8.0 ms claimed by the supplier [26].

Finally, Figure 18 shows the two-dimensional temperature distribution in the thermistor layer at two different elapsed times, 1 and 50 ms. This temperature distribution is computed by taking the mean temperature between the two planes of nodes constituting the mesh in the thermistor layer. The figure clearly shows that the active part of the flake is concentrated in the center ($1.5 < x < 3.5$ mm). At the far left and right edges the flake remains at a constant temperature whereas the center reveals relatively large variations between 1 ms and 50 ms. The influence of the spatial distribution of incident energy on the response of the instrument is reported in Section 4.2.

More accurate values for thermophysical properties were obtained after these preliminary results were shown to the Radiation Sciences Branch at NASA's Langley Research Center [33]. The temperature profiles in the active flake based on these property values are similar to the profiles in Figure 16. These values, given in Table

4, were used in all subsequent studies.

4.1.2 Results Using Realistic Thermophysical Properties

The following results take into account self heating in the thermistor and have been computed with the best available values for thermophysical properties. Figure 19 shows that when there is no radiative heat input the highest temperature is in the thermistor (bottom profile in Figure 19). Due to significant self heating the temperature there is about 2 K higher than in the heat sink. The absorber surface is a little cooler due to radiative heat loss through the telescope. As soon as a constant radiative heat flux illuminates the sensor the temperature rises. Also note that the temperature through the thermistor is essentially uniform. This is due to the relatively large thermal conductivity of the semiconductor material. After 20 ms the temperature distribution is for all practical purposes that of steady-state. Figure 20 shows the evolution with time of the average temperature in the thermistor. The thermal time constant of the thermistor is found to be 8.5 ms. Recall that according to the vendor the thermal time constant is supposed to be 8.0 ms [26].

4.2 Study of Equivalence

The concept of equivalence, or nonequivalence, refers to the effect that spatial distribution of a given power input to the instrument might have on the

instrument signal response. It is important to know whether or not sources of equal power which produce different nonuniform spatial distributions on the absorber flake are perceived by the instrument as identical. The working hypothesis of ERBE scientists has been to accept equivalence as a given characteristic of the thermistor bolometer radiometer. This hypothesis is tested in this thesis through several test cases.

4.2.1 Point Source versus Uniform Source Distributions

The two sources compared are of equal power, 10 mW. This is a typical value for the ERBE total scanning channel observing a daytime Earth scene. The power input to the detector from the point source is concentrated on a very small area. With a uniform source, the power input is uniformly distributed over the entire absorbing surface of the detector. While looking at space, the equilibrium temperature distribution in the active area of the thermistor is essentially uniform, as shown in Figure 21.

The equilibrium temperature distribution in the thermistor obtained with a 10-mW point source is shown in Figure 22. For this case all 10 mW are assumed incident to the surface corresponding to a single node. Heat is rapidly conducted from the absorbing surface to the thermistor layer. Even though the thermistor material has a high thermal conductivity, heat conduction in the horizontal plane is minimal due to the geometry. Therefore the temperature distribution shows a spatial

nonuniformity similar to that of the power input. The maximum temperature reached in the thermistor is about 5 K higher than the average temperature of 313.59 K.

The steady-state temperature distribution in the thermistor for the case of a 10-mW uniform source is shown in Figure 23. Here again the temperature increase has a spatial distribution similar to that of the power input; it is essentially uniform over the active part of the detector. The average temperature reached in this case is again 313.59 K, which is consistent since the power input is identical in the two cases.

The overall resistance of the thermistor, whose computation is described in Section 3.2.2, differs from one case to the other. Figure 24 shows the relationship between the overall resistance and the average temperature when this latter increases from its initial to its steady-state value for the two cases. For a given temperature the overall resistance of the thermistor is lower if it was heated by a point source than by a uniform source. This phenomenon characterizes a nonequivalent behavior of the instrument. This difference is detected through the output signal of the electronic circuit. The signal responses for both cases are shown in Figure 25. The final steady-state values differ from one another by 15 percent.

4.2.2 Rotation of a Spatially Nonuniform Source Distribution

The present test case involves a source whose spatial distribution on the

absorber surface of the detector, while still rather extreme, is more representative of an Earth scene. The spatial distribution of the energy incident to the detector is inspired from a result in reference 21 which is reproduced in Figure 26. The distribution from reference 21 has been scaled up so that it covers the active area of the flake. The response to this source is compared to that for an identical source rotated 45 deg on the absorbing surface. The power input is again 10 mW in both cases. The final temperature distributions are shown in Figures 27 and 28. The shape of this distribution is closely related to the spatial distribution of the incoming flux, again because of the predominant heat conduction through the flake. The final average temperature in both cases is 313.59 K, as expected. The overall resistance of the thermistor layer is found to be almost identical in both cases, about 117 k Ω , the difference being less than 5 Ω . This difference is detected and amplified by the electronic circuit. The difference in the steady-state signal response of the instrument, shown in Figure 29, is only 0.05 percent, which is too small to be seen in the figure.

4.2.3 Equivalence versus Nonequivalence

Equivalence of an instrument such as the thermistor bolometer radiometer is an important concept since Earth scenes of identical power are likely to have different spatial distributions. The first test case, involving the point and uniform sources, seems to reject the equivalence assumption, whereas the second more realistic test case validates the hypothesis. It is important to realize that the first

test case is highly unrealistic and not at all representative of typical Earth scenes. However, it would be interesting to compare instrument responses corresponding to an internal calibration and a typical Earth scene, which may have significantly different spatial distributions. Nonequivalence might be an issue which should be taken into account as a possible bias of the instrument in this case. The second more realistic test case shows that the instrument is probably not sensitive to the type of differences in Earth radiation fields that would typically be encountered in practice.

4.3 Earth Scan Simulation

A geographical scene sequence is now imagined in which the radiometer scans across different source types on Earth. This scene sequence corresponds to a typical situation when the Earth Radiation Budget spacecraft crosses the equator 22.5° East of the noon time meridian [34]. This scene is sketched in Figure 30.

The radiometer scans from left to right as the satellite crosses the equator. At the far left the instrument looks at space, and as it scans toward the right it sees successively the ocean, a cloud bank, some more ocean, a jungle, and finally a desert scene before going off the edge of the Earth for another space look. The sensor then rotates all the way up into the spacecraft for internal calibration before performing the return scan. This typical scan, which occurs as the spacecraft

moves in a direction perpendicular to the scan direction, takes 3.5 s.

The power input to the bolometer in milliwatts from each scene is represented in Figure 31. Note that the transitions from one feature to the next are assumed to be instantaneous. In reality the field-of-view of the instrument would cover parts of two adjacent features and the transition from one feature to the next would be more gradual. In addition, the power input of each feature was considered to be constant. Figure 32 shows the signal response in volts of the instrument electronics. The response matches the radiative input very closely except at the abrupt scene transitions when the small time delays of the electronics can be seen as rounding off of the response curve.

An experimental relation between radiative input and signal response is derived from the steady-state data. The relation shown in Figure 33 expresses the expected linear behavior of the instrument.

5.0 Conclusions and Recommendations

5.1 Conclusions

The following conclusions can be drawn from the results presented in this thesis:

1. A dynamic electrothermal model of the active flake of a scanning thermistor bolometer radiometer has been formulated that reveals the sensitivity of the temperature distribution in the flake to its dimensions and thermophysical properties.
2. The model shows that a one-dimensional lumped model could accurately predict the temperature profile through the thermistor bolometer. However, the three-dimensionality of the current model is necessary to study the influence of spatial distribution of radiation incident to the absorber.
3. The thermal time constant of 8.5 ms obtained by using the model confirms

the value of 8.0 ms claimed by the vendor.

4. The electronic analysis reveals the role of self heating in the active and reference flakes, and verifies that self heating must be considered in the thermal model.
5. The difference in channel signal response between a point source and a uniform source of identical power incident to the active flake is as high as 15 percent.
6. In the more representative case of rotation of a nonuniform radiative input distribution incident to the bolometer, the signal response changed by only 0.05 percent. Therefore, the hypothesis of equivalence is justified for viewing typical Earth scenes.
7. Dynamic simulation of Earth scanning has been successfully performed, indicating the value of the current model as a component of an eventual end-to-end model.

5.2 Recommendations

1. The dynamic electrothermal model of the active flake should be linked to the optical model of reference [21] and a dynamic thermal model of the radiometer housing such that the power input distribution to the flake model is computed by the optical model, and the evolution of the heat sink and other component temperatures is correctly accounted for. The result would

be a true "end-to-end" model of the instrument.

2. A FORTRAN version of the electronic model should be developed to make possible a direct linkage between the electronic and electrothermal models. The commercial software PSpice® should be used to verify the new electronic model.
3. Simulations should be run using the end-to-end model to evaluate the equivalence under representative Earth scanning and internal calibration conditions.
4. The equivalence of the instrument to calibration sources and typical Earth scenes should be verified. This would require a model for the calibration sources.

Table 1. The Suite of Instruments Carried by Each Satellite

Spacecraft	Launch Date	Instrument Type	Field-of-View (Resolution)	Channel Spectral Range (μm)
ERBS	8 October 1984	Scanning Radiometer	Narrow (about 30 km)	Shortwave (0.2-5.0)
				Longwave (5.0-50.0)
				Total (0.2-100.0)
NOAA-9	12 December 1984	Non-scanning Radiometer	Medium (about 1000 km)	Shortwave (0.2-3.5)
				Total (0.2-50.0)
NOAA-10	17 September 1986		Wide (entire Earth disk)	Shortwave (0.2-3.5)
				Total (0.2-50.0)

Table 2. Thicknesses of the Layers of the Detector Flake.

Layer	Thickness (μm)	Horizontal Dimensions (mm)
Absorber	10.6	1.5 x 1.5
Bond/Sealant	7.5	3.0 x 1.5
Gold Bus	0.5	3.0 x 1.5
Thermistor	12.0	3.0 x 1.5
Bond	3.0	3.0 x 1.5
Kapton	7.6	3.0 x 1.5
Bond	3.0	3.0 x 1.5
Total	44.2	

Table 3. Components Used in the Detector Circuit and Their Values.

Symbol	Device Description	Value
Vb	Bias Voltage	± 86 V
R1	Resistance of Active Flake	Variable
R2	Resistance of Reference Flake	Variable (≈ 117 k Ω)
R3	Resistance of Bridge Resistor	75.301 k Ω
R4	Resistances of Bridge Resistors	75.121 k Ω
Ra & Rb	Ballast Resistors	4 k Ω
R5 & R6 & Rd	Resistors	511 & 274 & 10 k Ω
R7	Feedback Resistor	935 k Ω
C1 & C2	Capacitors	220 & 470 pF
OP07A	Operational Amplifier	-
Vs	Voltage Supply to Op Amp	± 22 V
Vp	Output Voltage	Variable [0,22V]

Table 4. Nominal Values of the Thermophysical Properties Used in the Electrothermal Model of the Thermistor Bolometer Flake.

	Thermal Conductivity (W/m-K)	Specific Gravity	Specific Heat (J/kg-K)
Absorber	0.209	1.40	668.8
Bond/Sealant	0.104	1.15	1000 (?) [*]
Gold Bus	315.0	19.32	129.2
Thermistor	8.360	5.00	752.4
Bond	0.104	1.15	1000 (?)
Kapton	0.120	1.42	1091
Bond	0.104	1.15	1000 (?)

* Question mark (?) represents uncertainty in the nominal value.

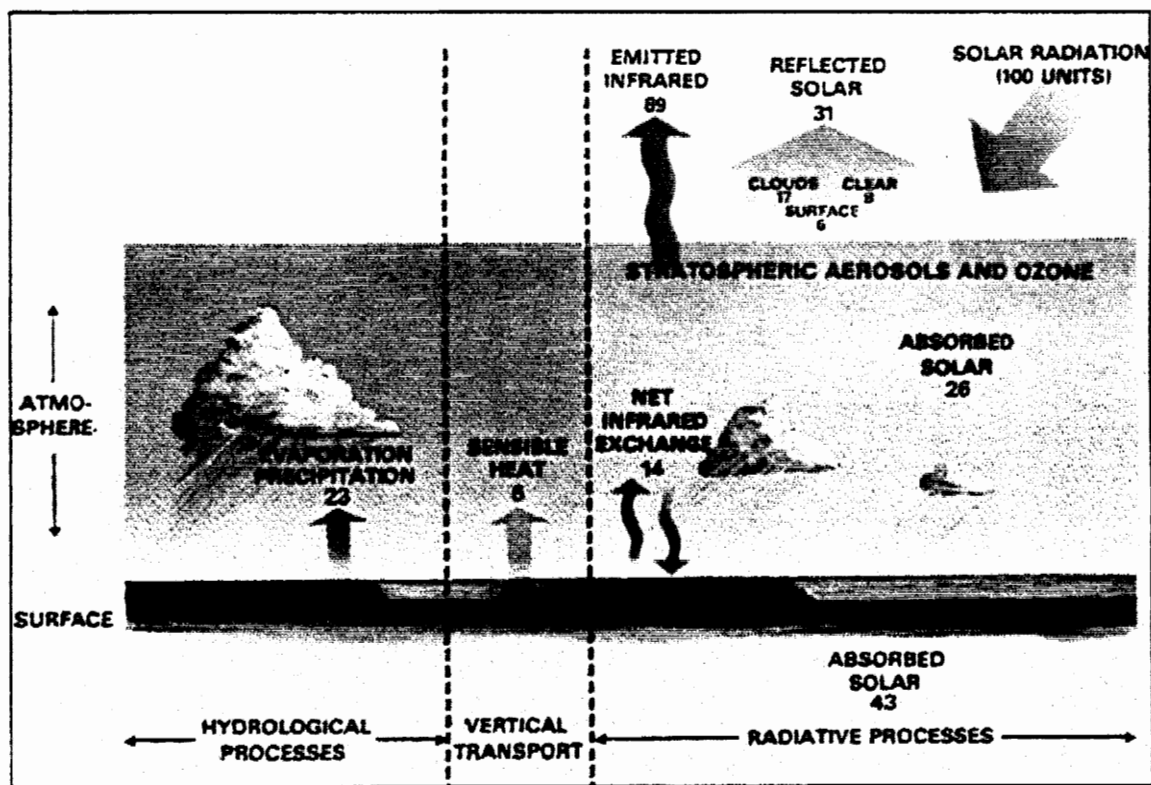


Fig. 1 Processes Contributing to the Radiation Balance of the Earth and its Atmosphere (Courtesy of NASA Goddard Space Flight Center).

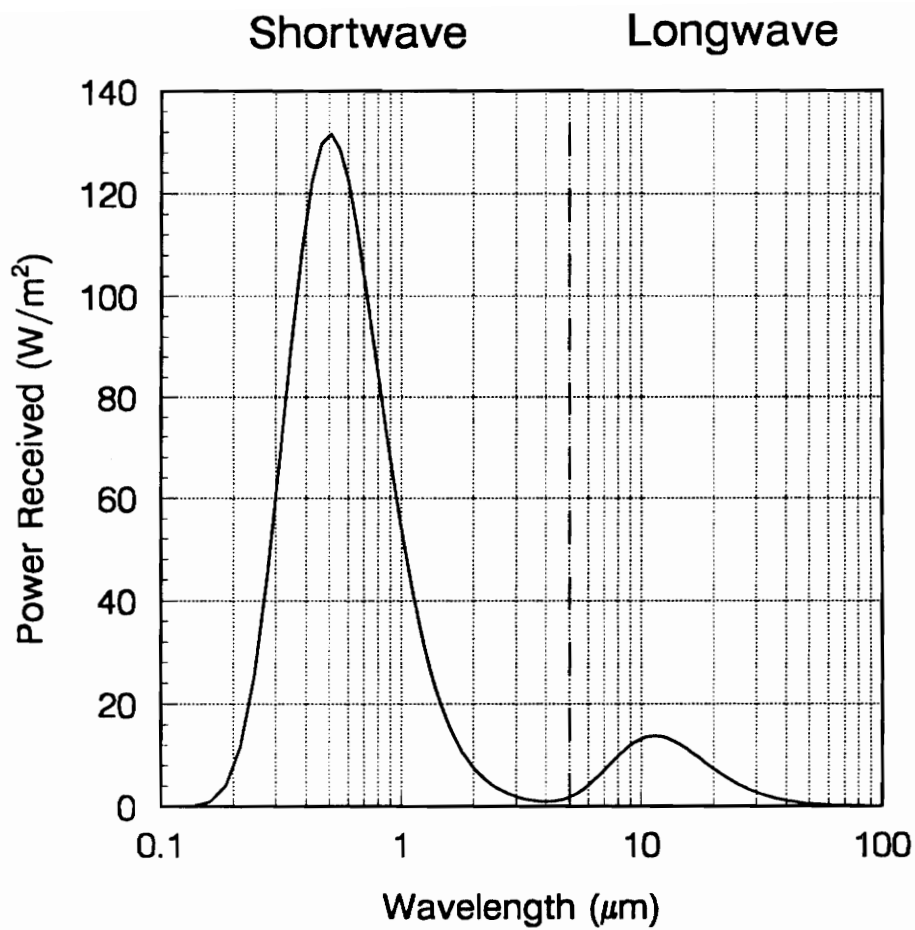


Fig. 2 Representative Spectrum of Typical Daylight Earth Scene.

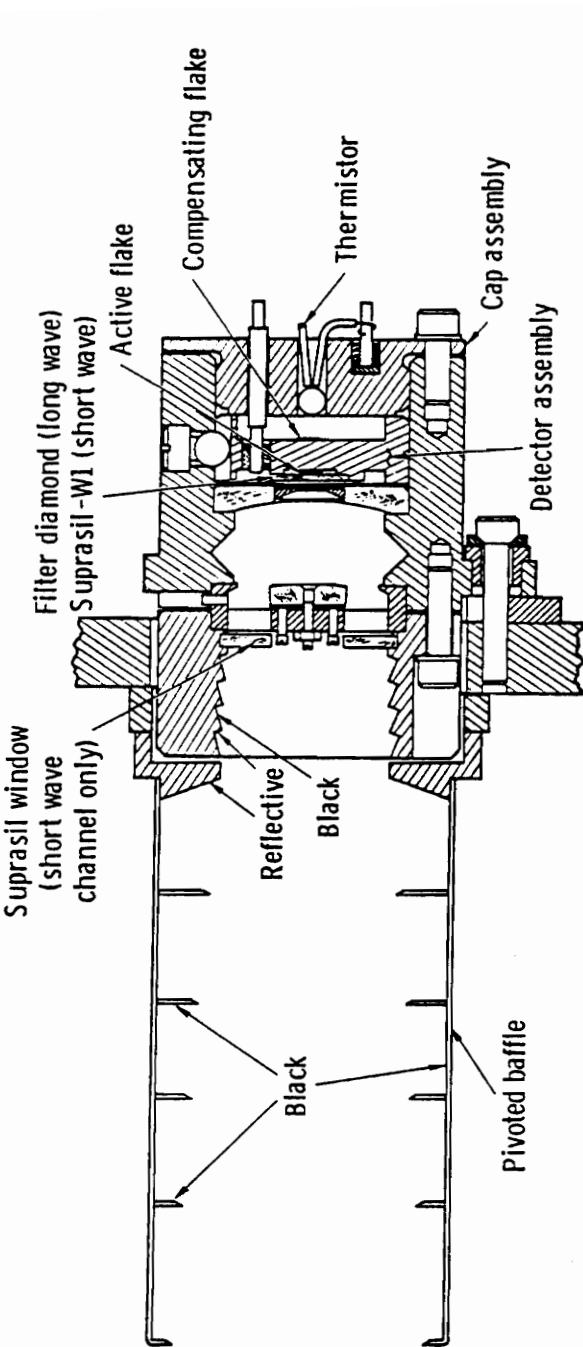


Fig. 3 The ERBE Scanning Radiometer Telescope (Courtesy of NASA Langley Research Center).

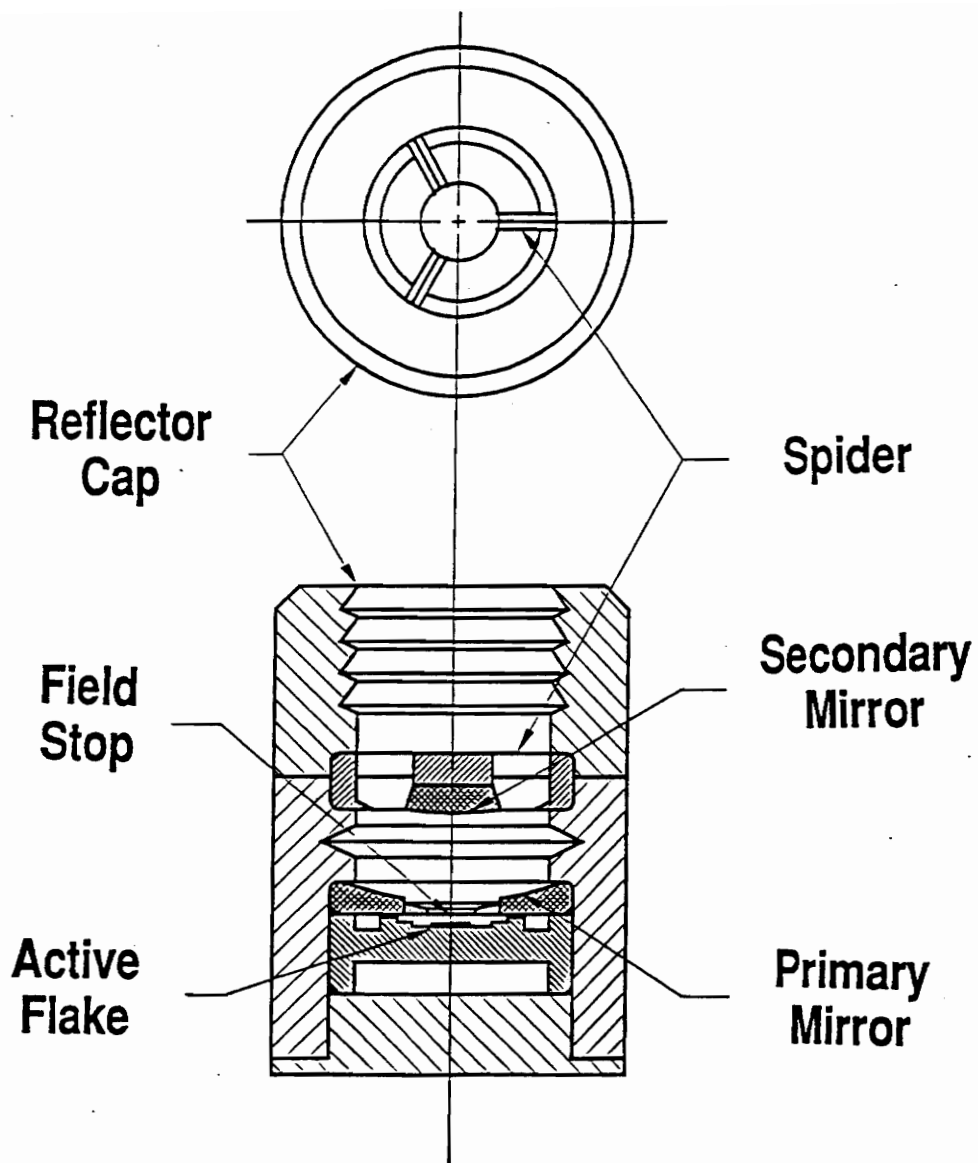


Fig. 4 Meekins' Model of the ERBE Scanning Channel [21].

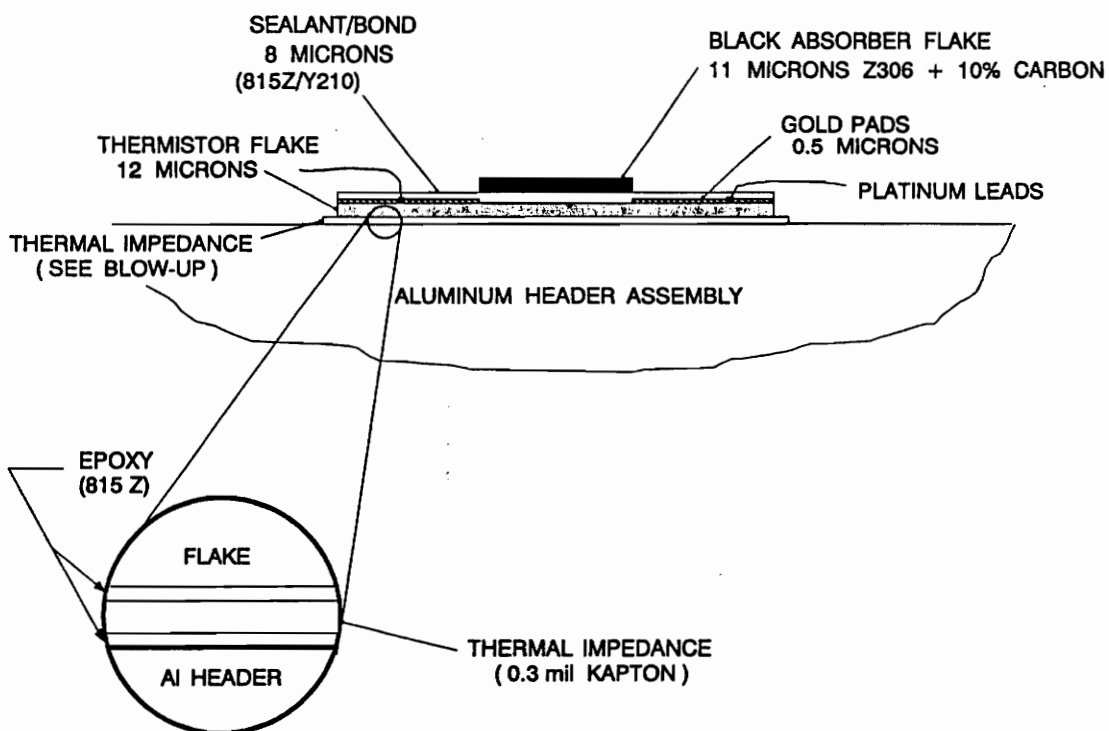


Fig. 5 Thermistor Bolometer Construction [26].

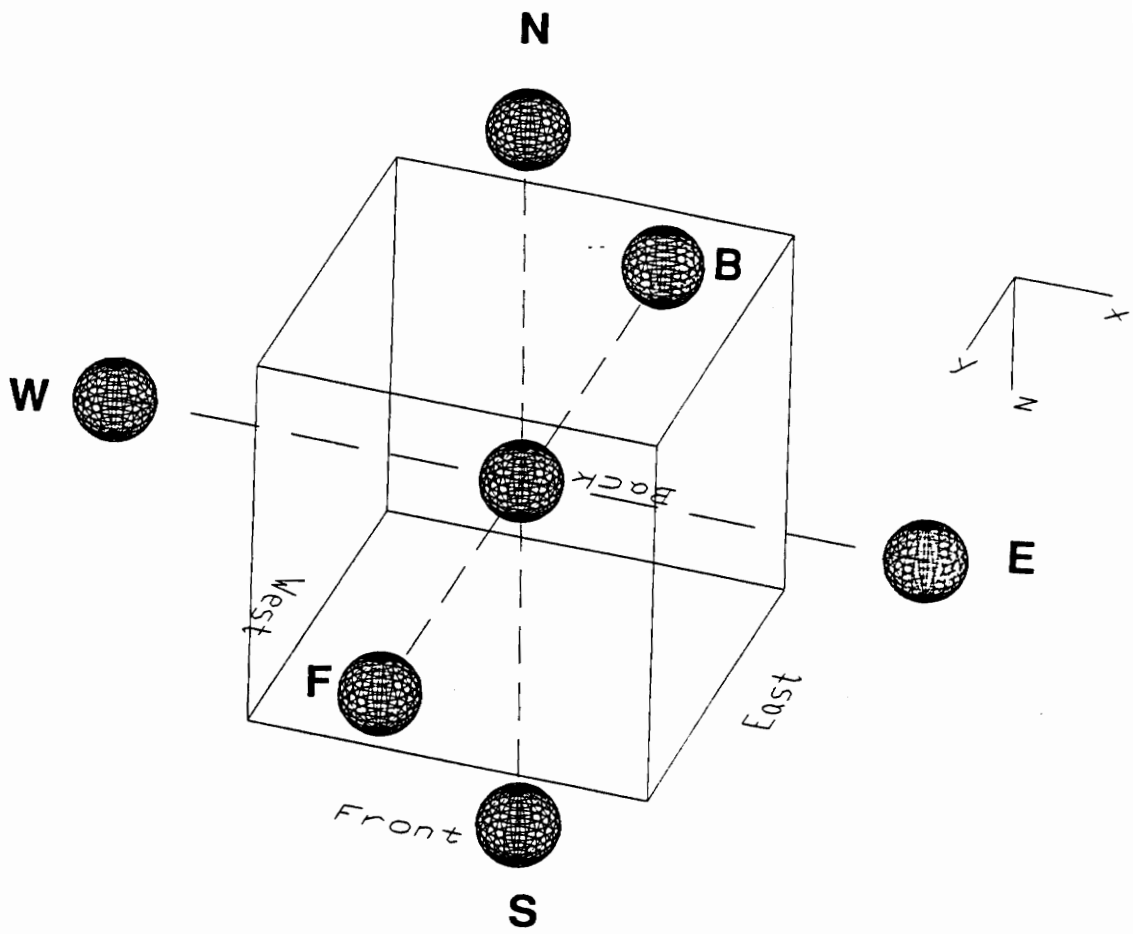
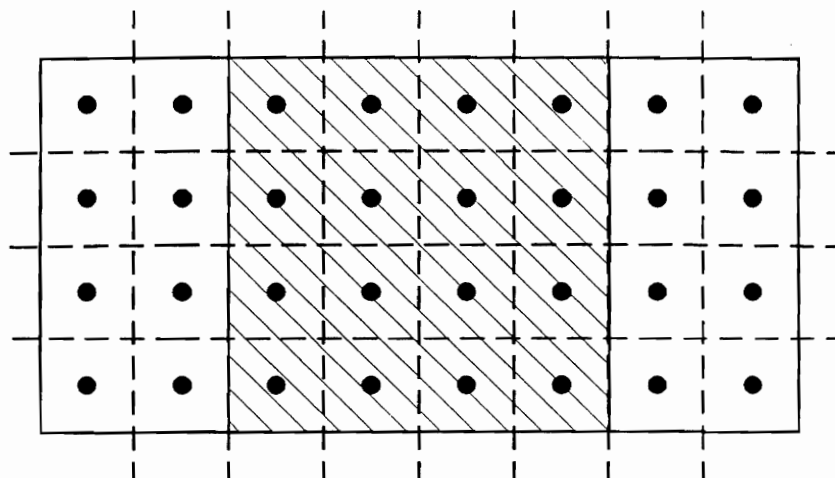
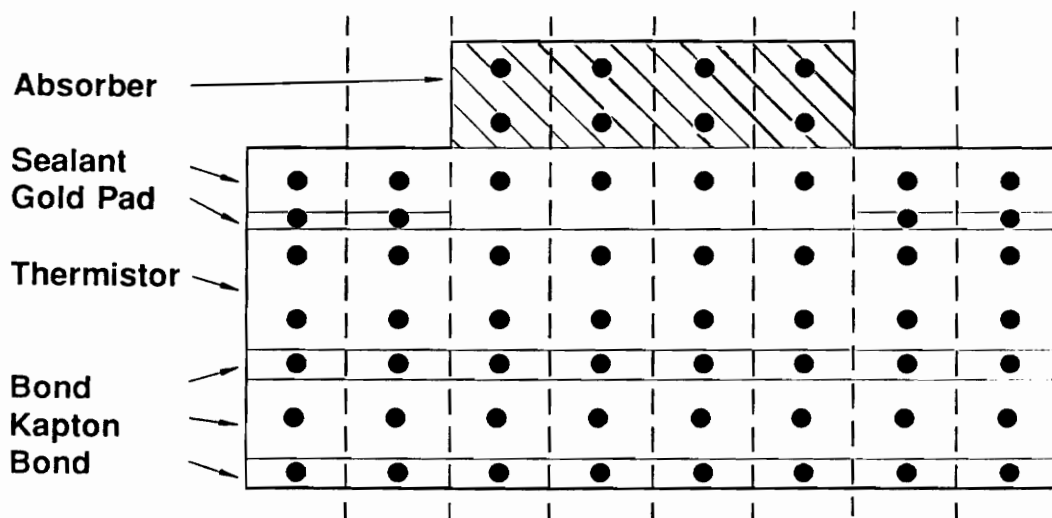


Fig. 6 Finite Difference Volume Element.



(a)



(b)

Fig. 7 Finite Difference Node Mesh for the Active Flake Thermal Model; (a) Plan View and (b) Front Elevation.

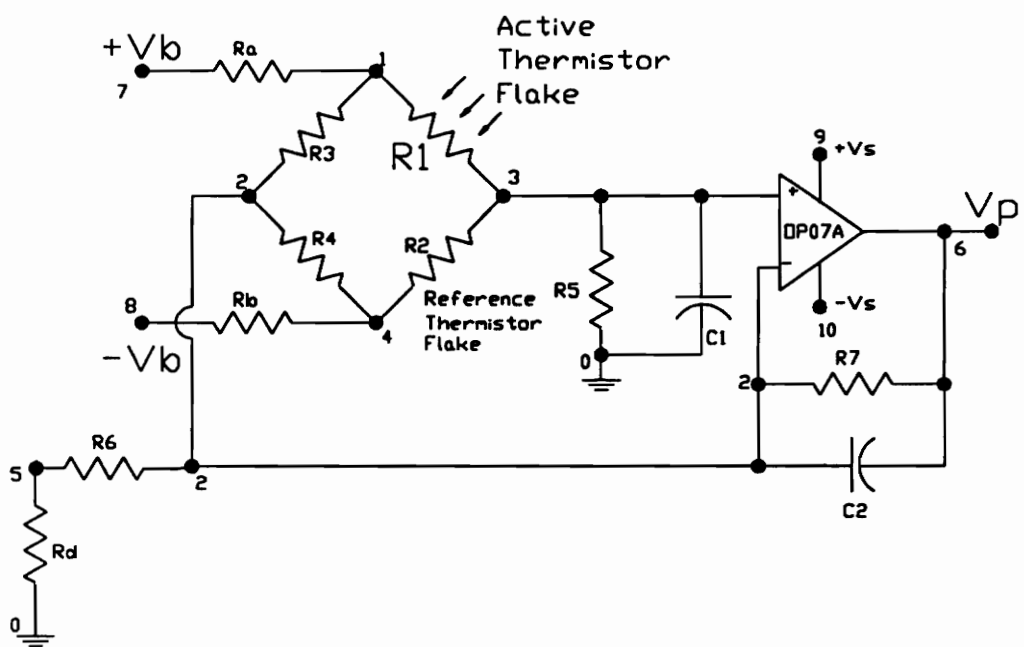


Fig. 8 Detector Bridge Amplifier Circuit [29].

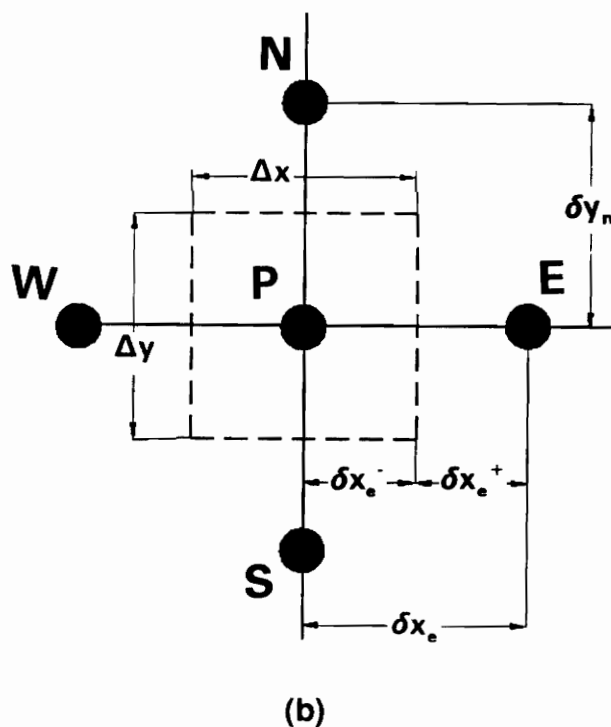
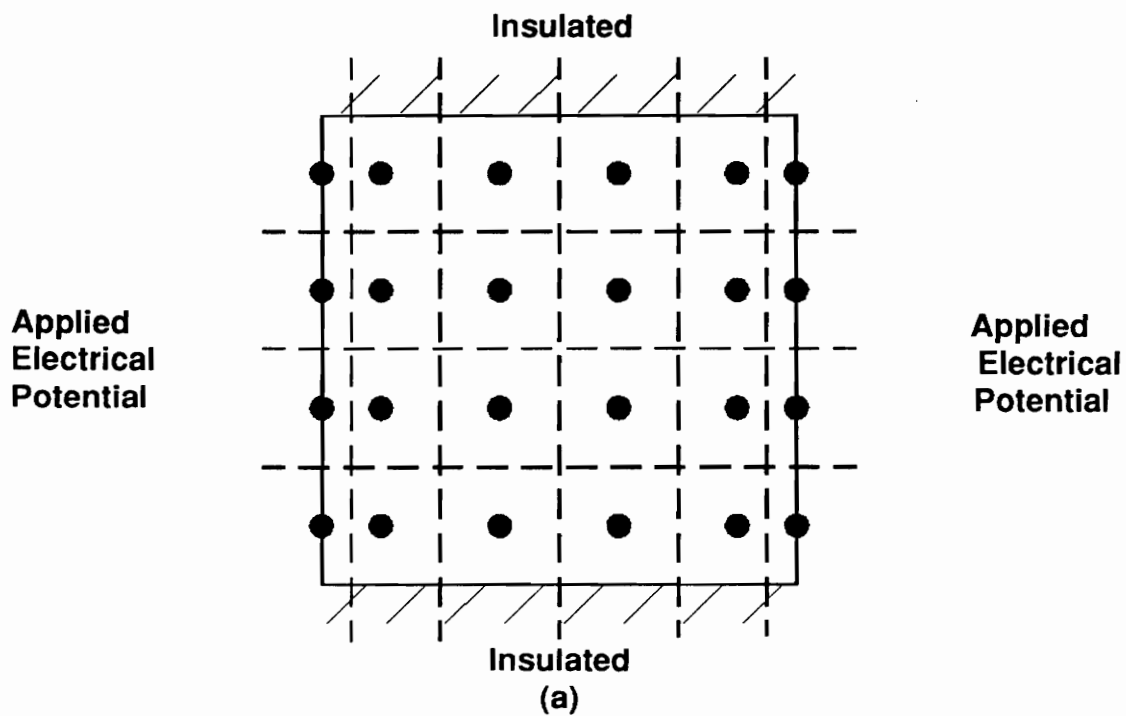


Fig. 9 (a) Finite-Difference Node Mesh for the Electrical Model and (b) Control Volume Element for Two-Dimensional Finite-Difference Mesh.

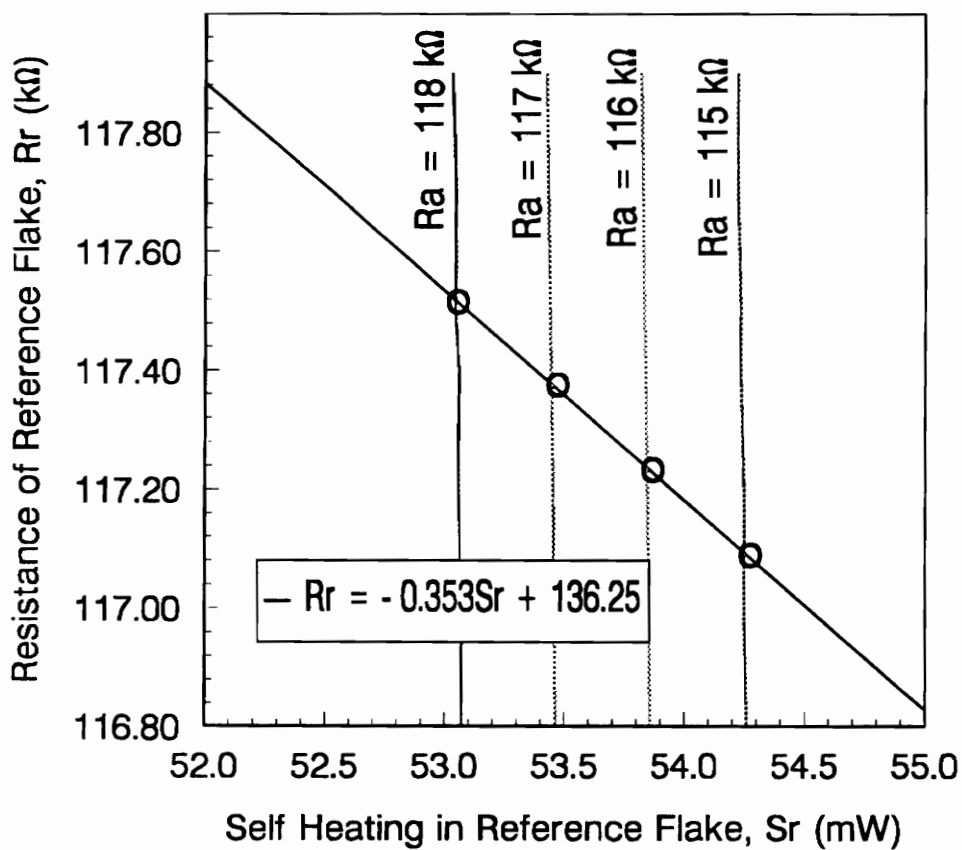


Fig. 10 Correlations Between Self Heating and Resistance in the Reference Flake.

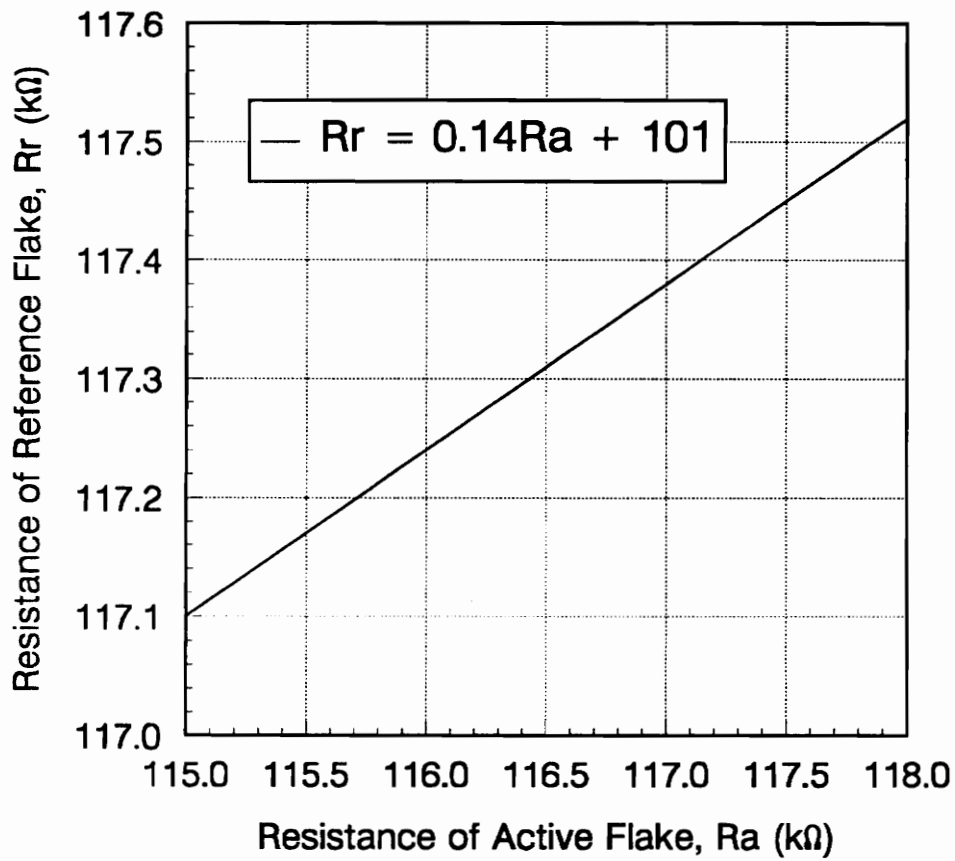


Fig. 11 Correlation Between Resistance of the Active Flake and Resistance of the Reference Flake.

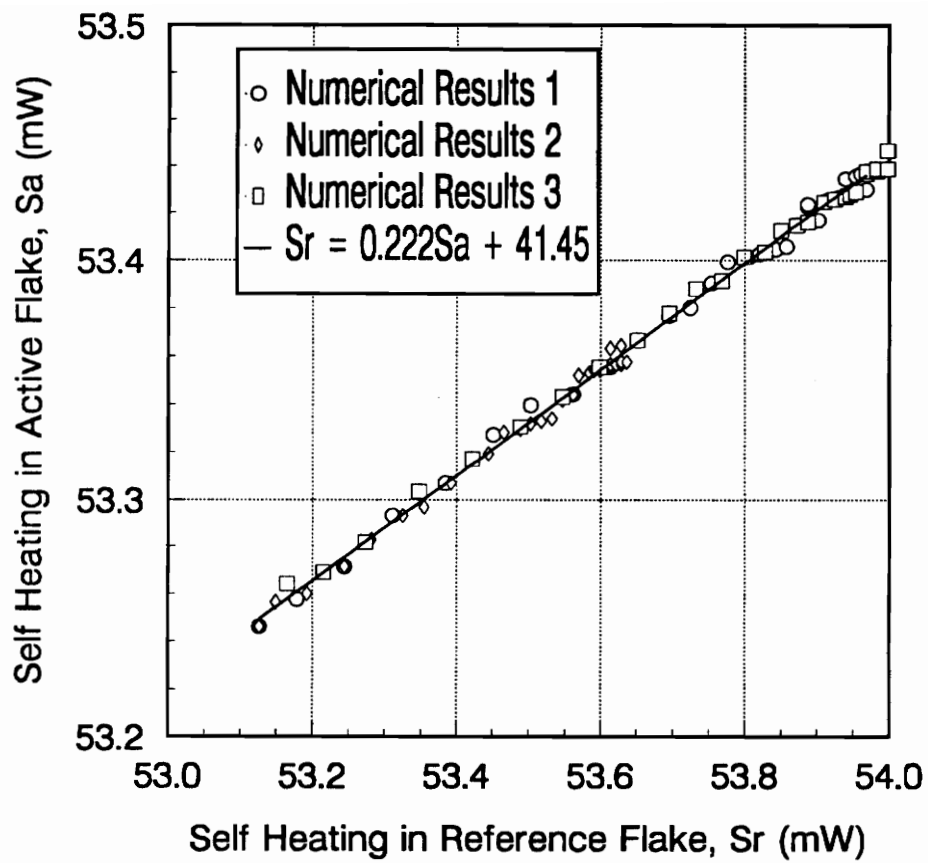


Fig. 12 Numerical Results and Correlation Between Self Heating in the Reference Flake and Self Heating in the Active Flake.

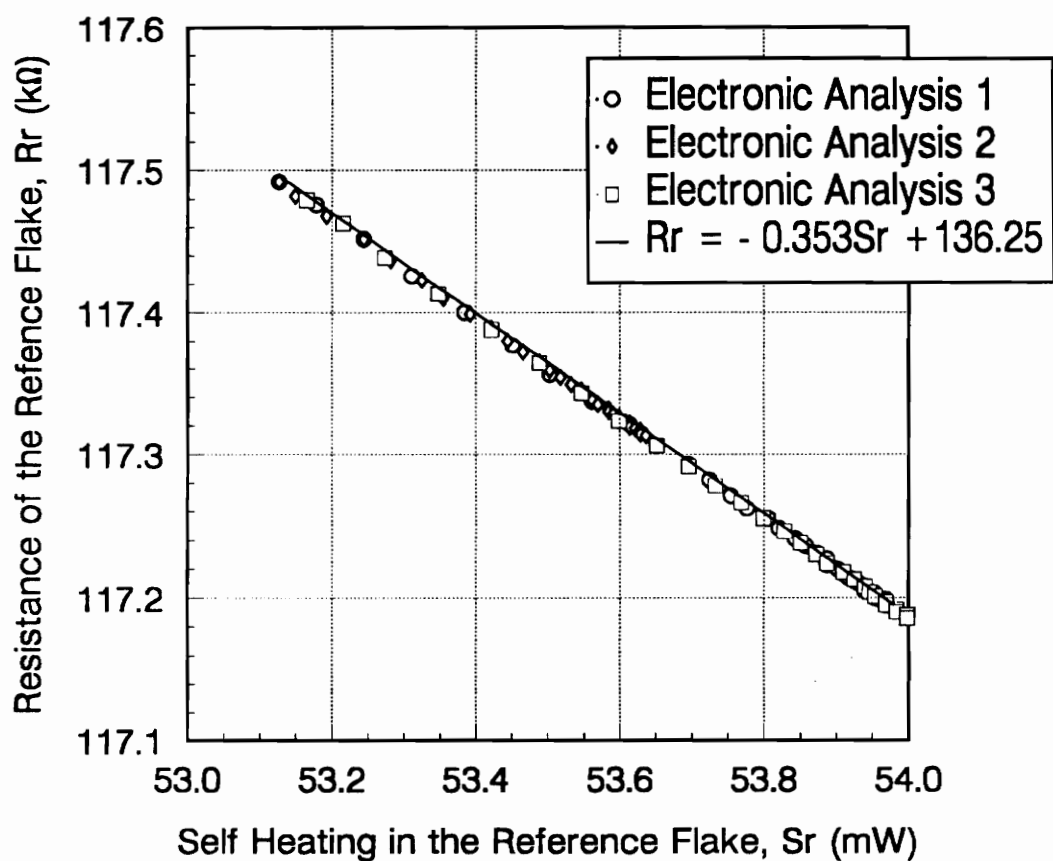


Fig. 13 Agreement of Electronic Analysis and Thermal Model for Correlation between Self Heating and Resistance in the Reference Flake.

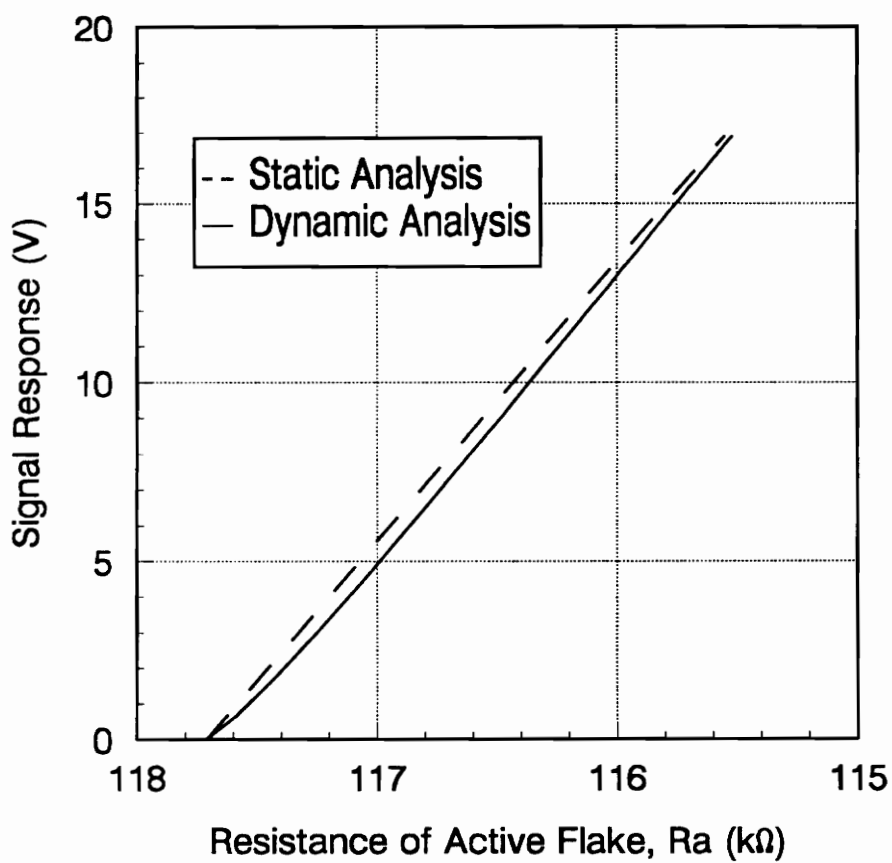


Fig. 14 Electronic Output as a Function of the Resistance of the Active Flake in Static and Dynamic Operation.

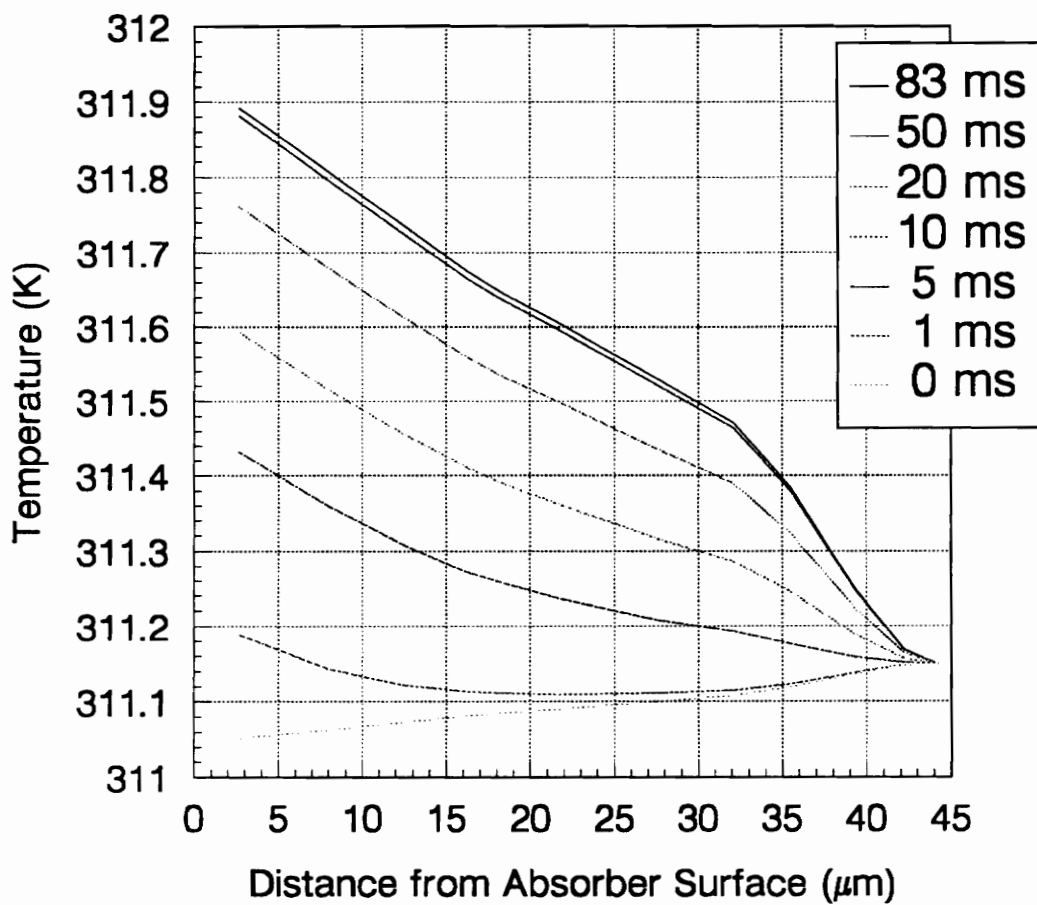


Fig. 15 Evolution with Time of the Temperature Profile Through the center of the Active Flake (Thermal Conductivity of the Thermistor 0.1 W/m-K).

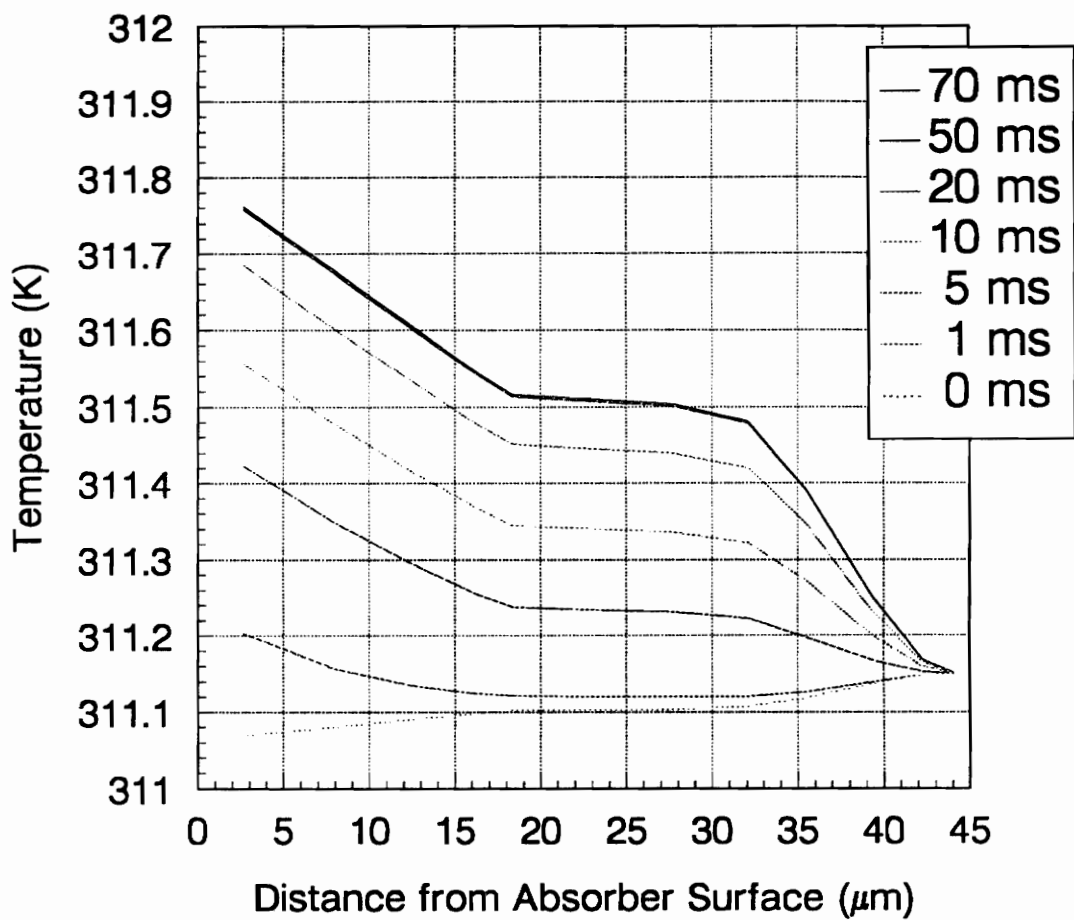


Fig. 16 Evolution with Time of the Temperature Profile Through the center of the Active Flake (Thermal Conductivity of the Thermistor 1.0 W/m-K).

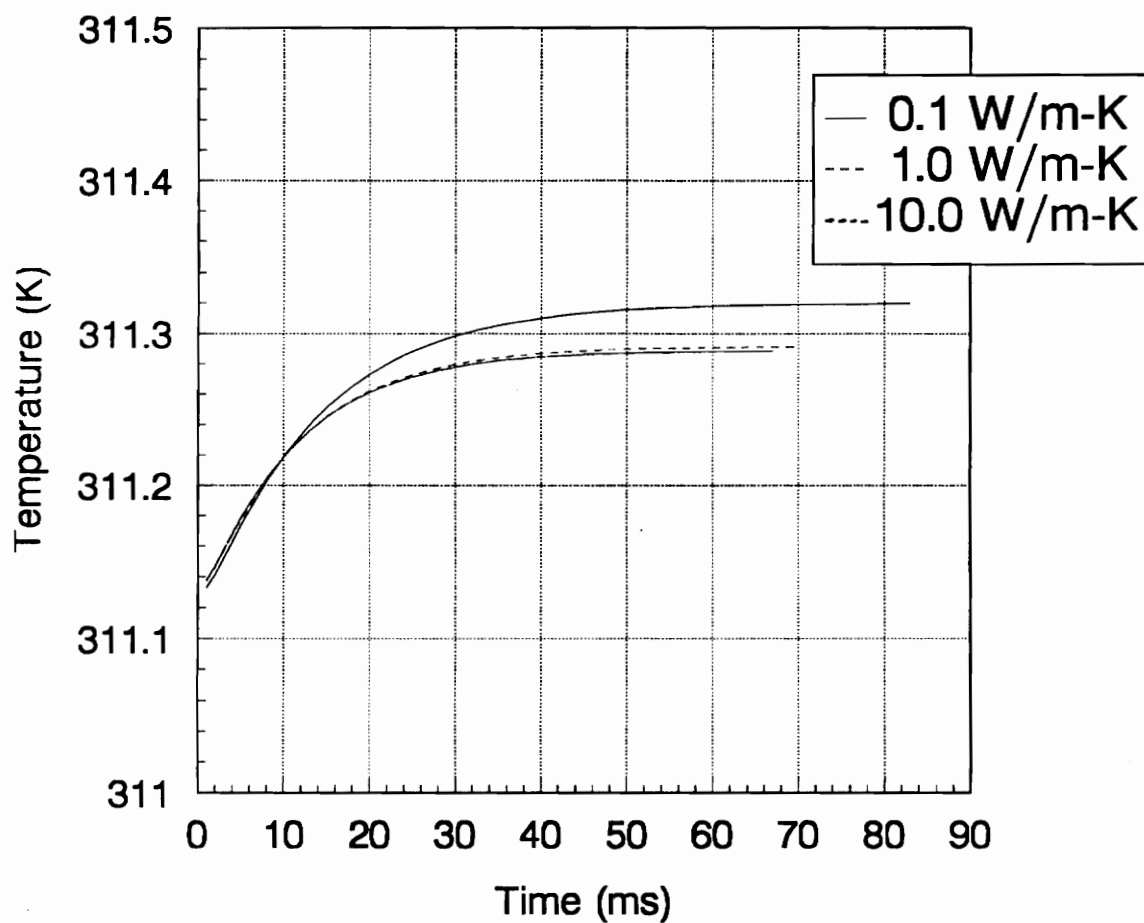


Fig. 17 Evolution with Time of the Average Thermistor Temperature.

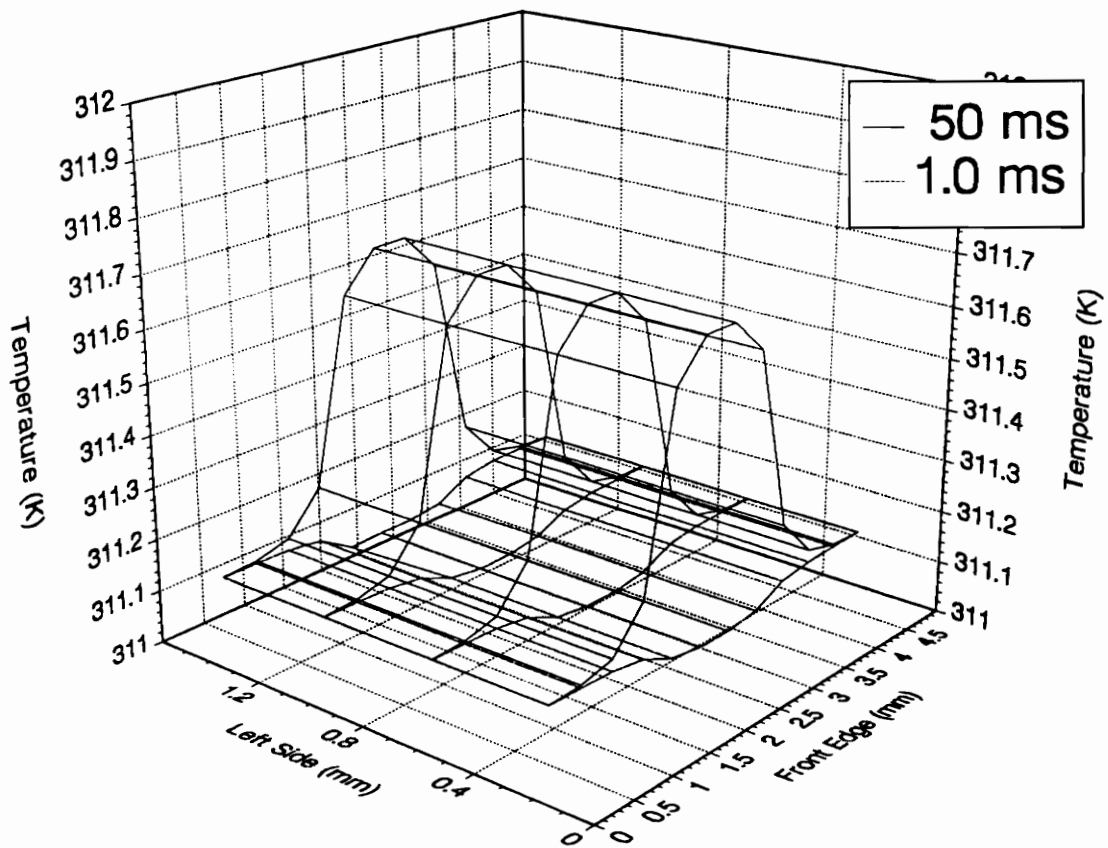


Fig. 18 Evolution with Time of the Two-Dimensional Temperature Distribution in the Thermistor.

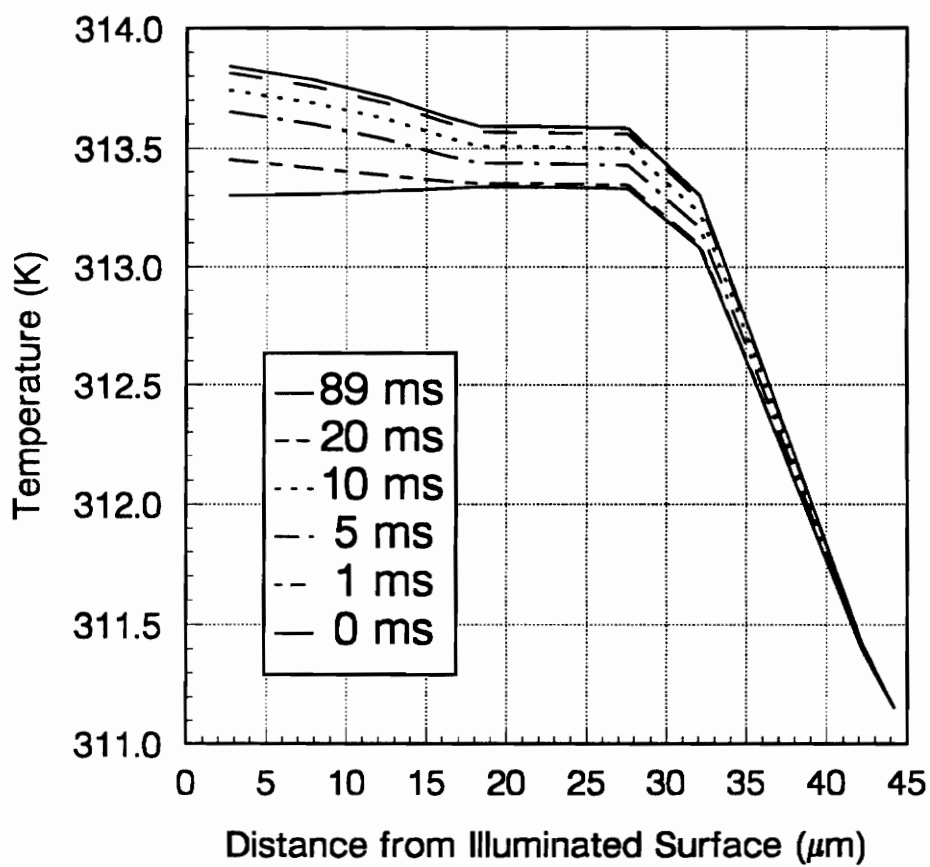


Fig. 19 Evolution with Time of the Temperature Profile Through the Active Flake with Self Heating and a 10-mW Radiative Power Input.

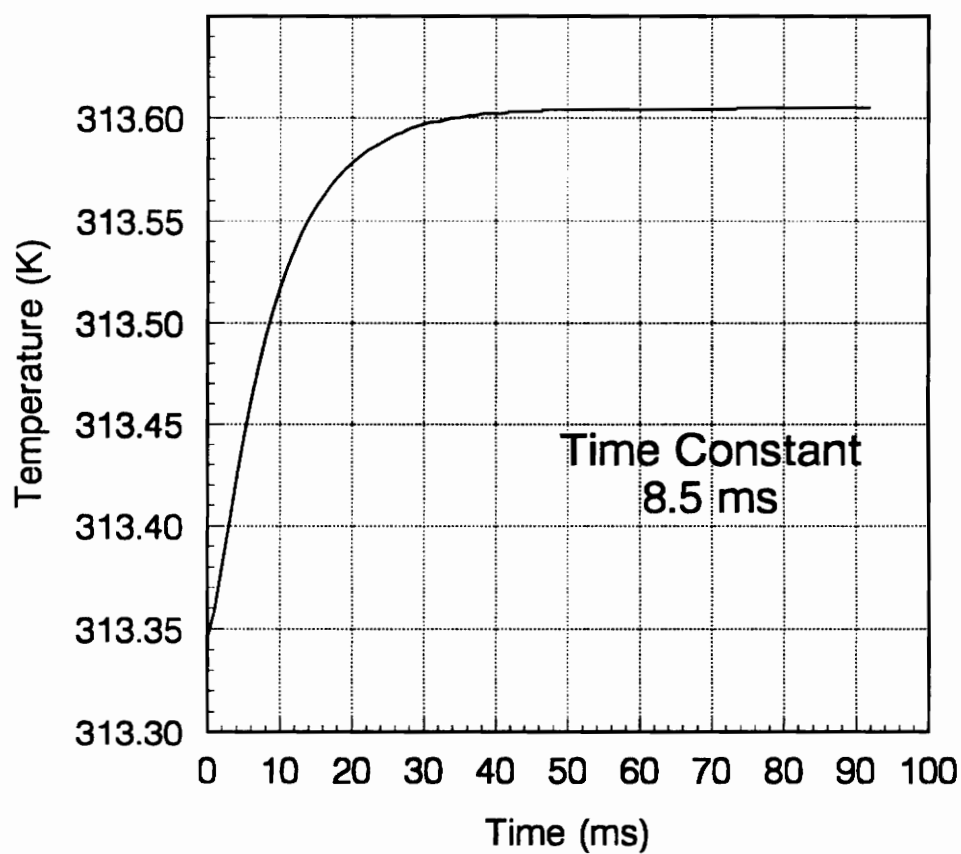


Fig. 20 Evolution with Time of the Average Thermistor Temperature (10-mW Radiative Power Input).

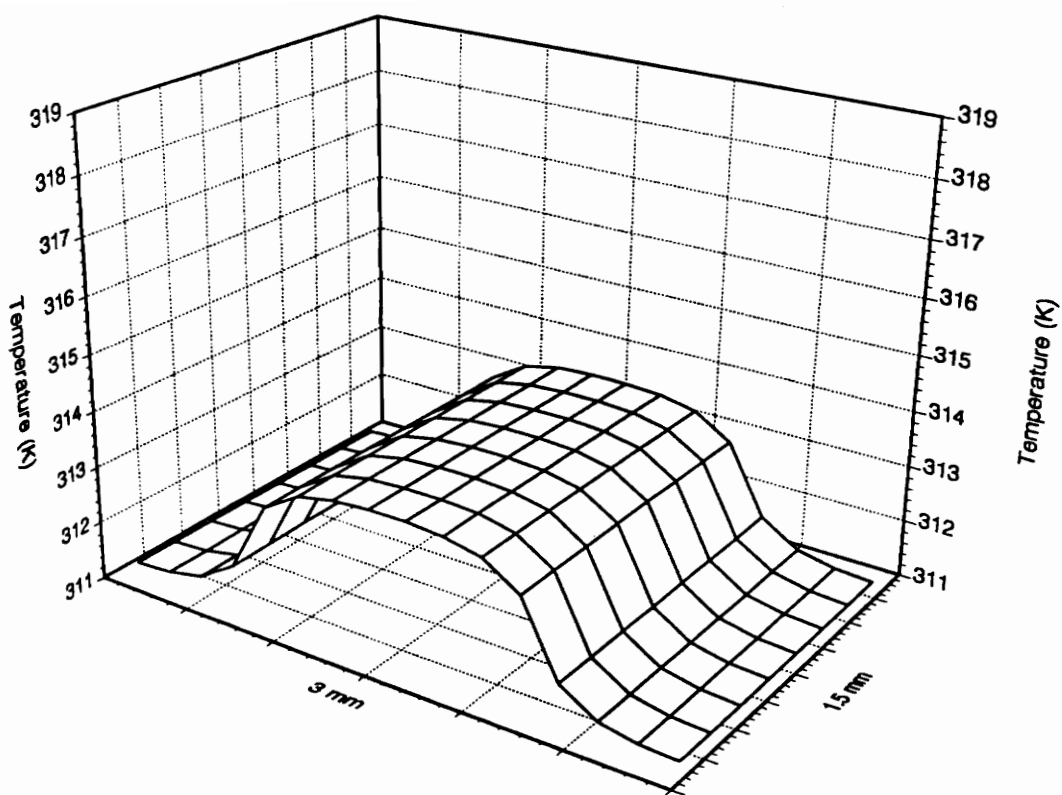


Fig. 21 **Equilibrium Two-Dimensional Temperature Distribution in the Thermistor During a Space Look.**

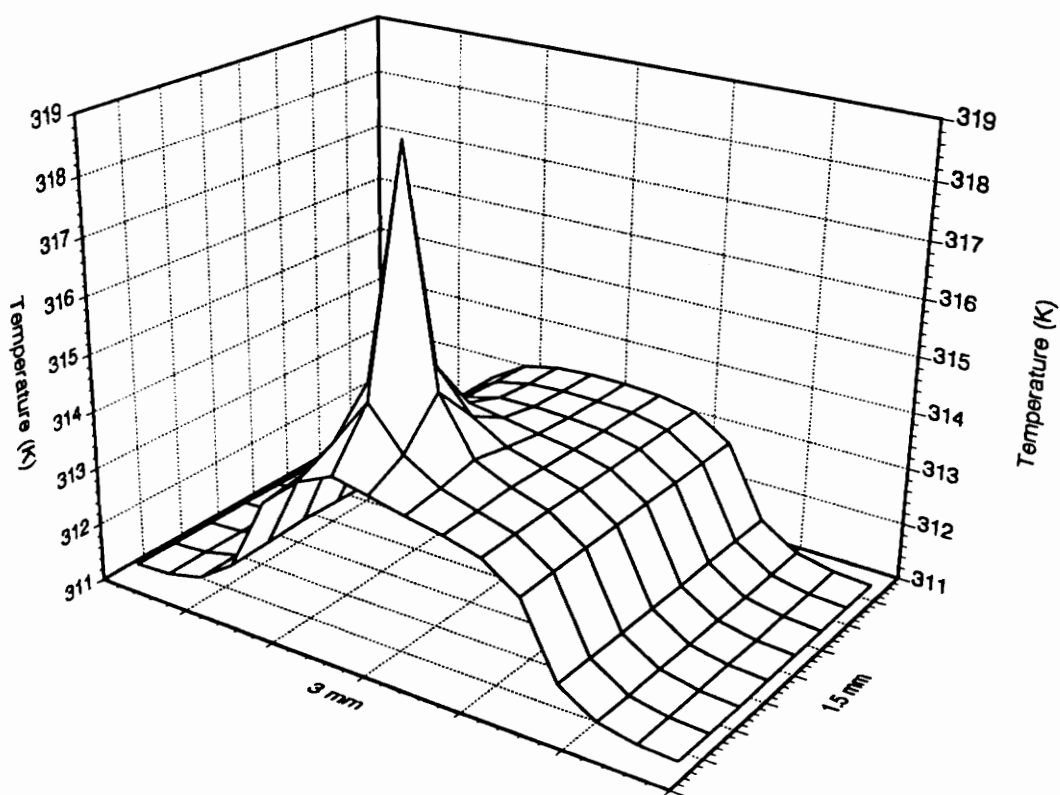


Fig. 22 **Equilibrium Two-Dimensional Temperature Distribution in the Thermistor for a 10-mW Point Source Power Input.**

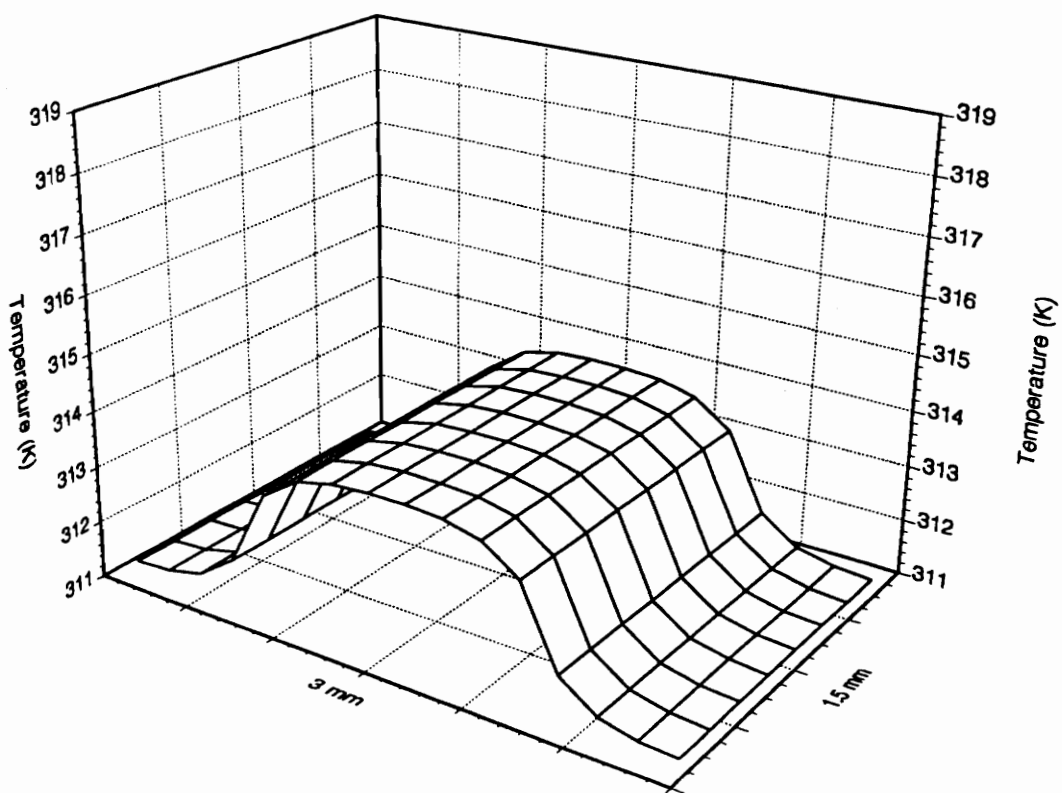


Fig. 23 **Equilibrium Two-Dimension Temperature Distribution in the Thermistor for a 10-mW Uniform Source Power Input.**

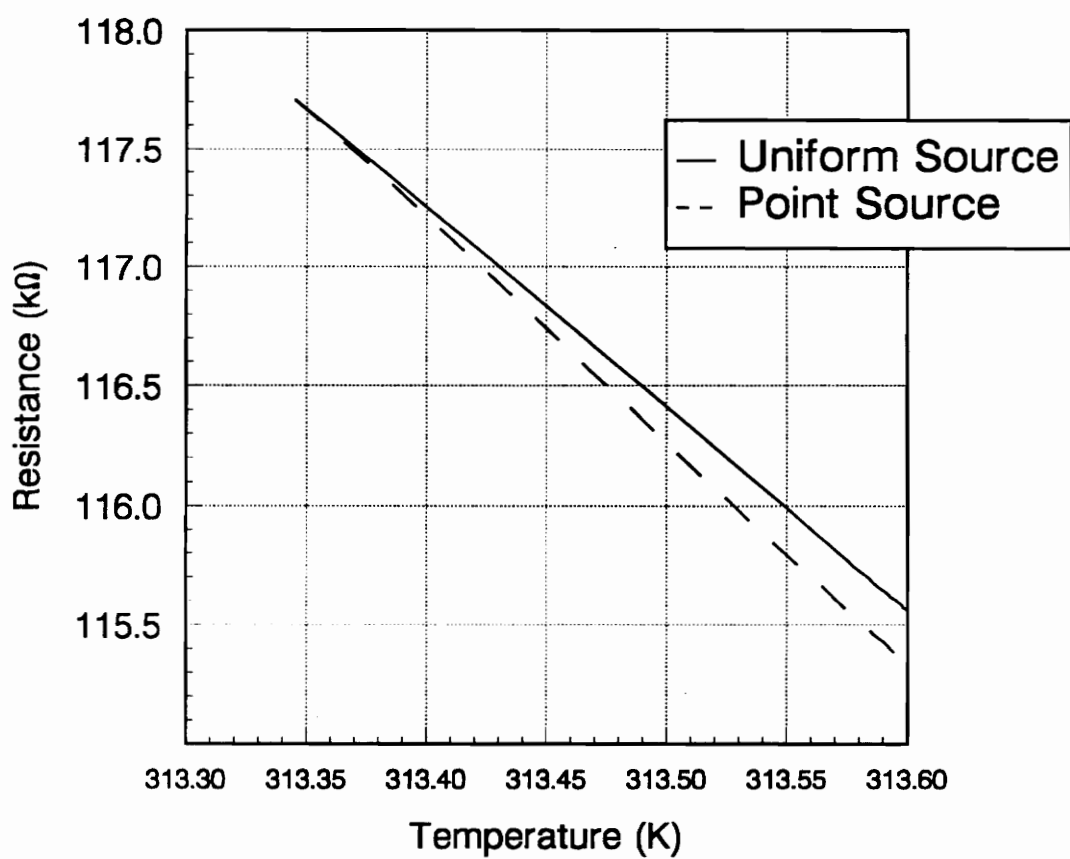


Fig. 24 **Relation Between Resistance and Temperature in the Active Flake during Illumination of the Sensor by a 10-mW Uniform Source and by a 10-mW Point Source Power Input.**

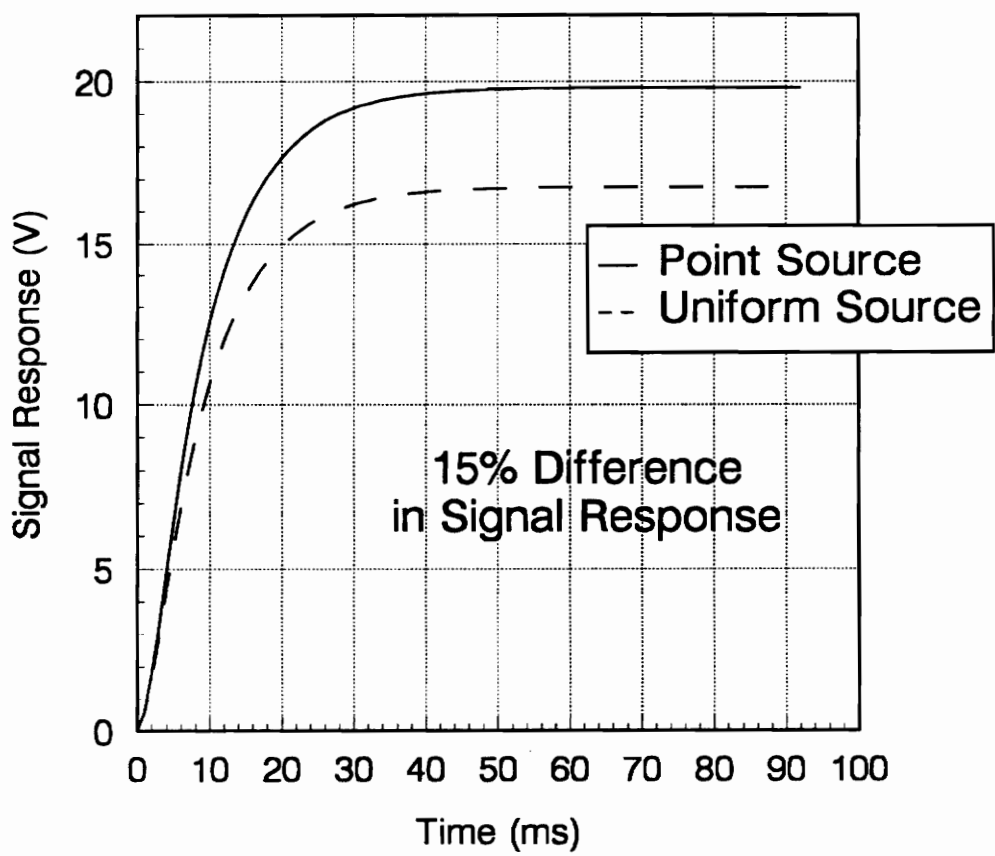


Fig. 25 Electronic Output as a Function of Time for a 10-mW Uniform Source and a 10-mW Point Source Power Input.

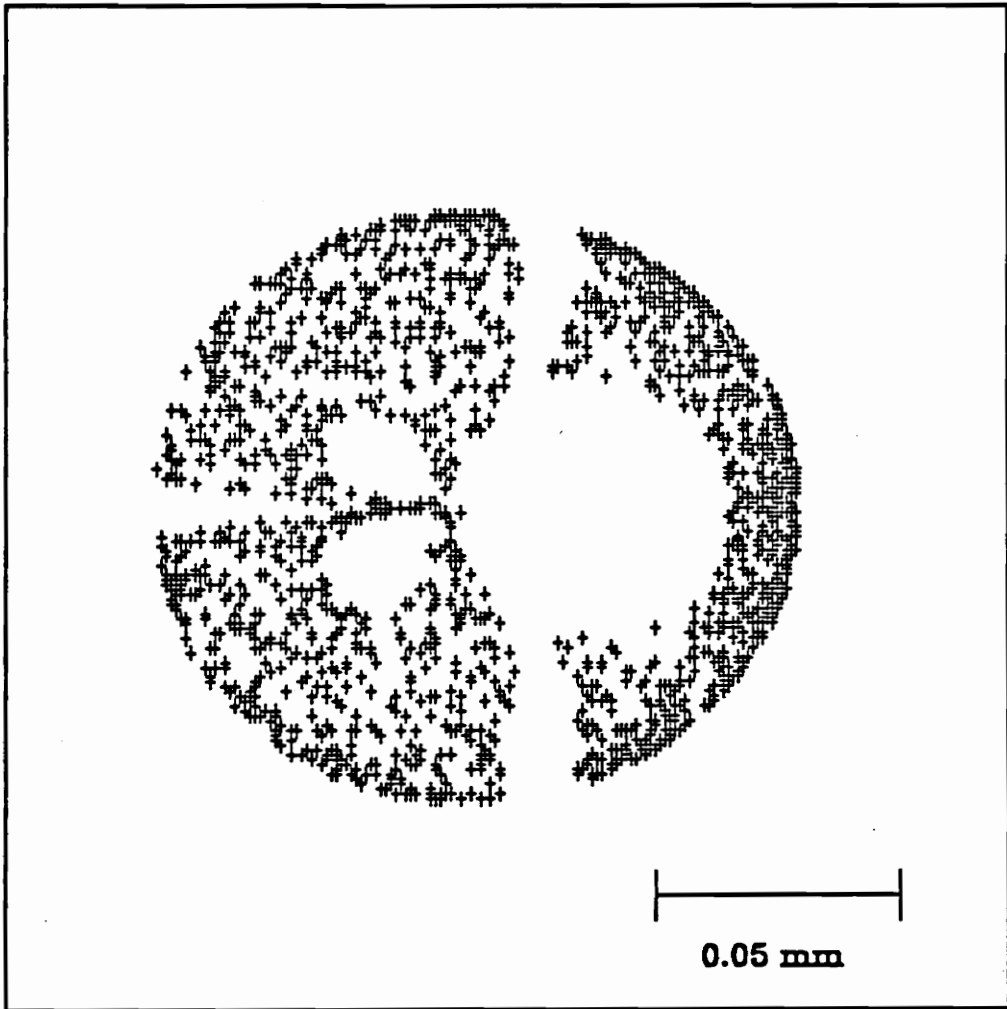


Fig. 26 **Radiation Distribution on the Active Flake for Collimated Radiation Incident to the Instrument Aperture at an Angle of 1.5 deg for which 33.4 percent of energy incident to instrument aperture reaches the flake [21].**

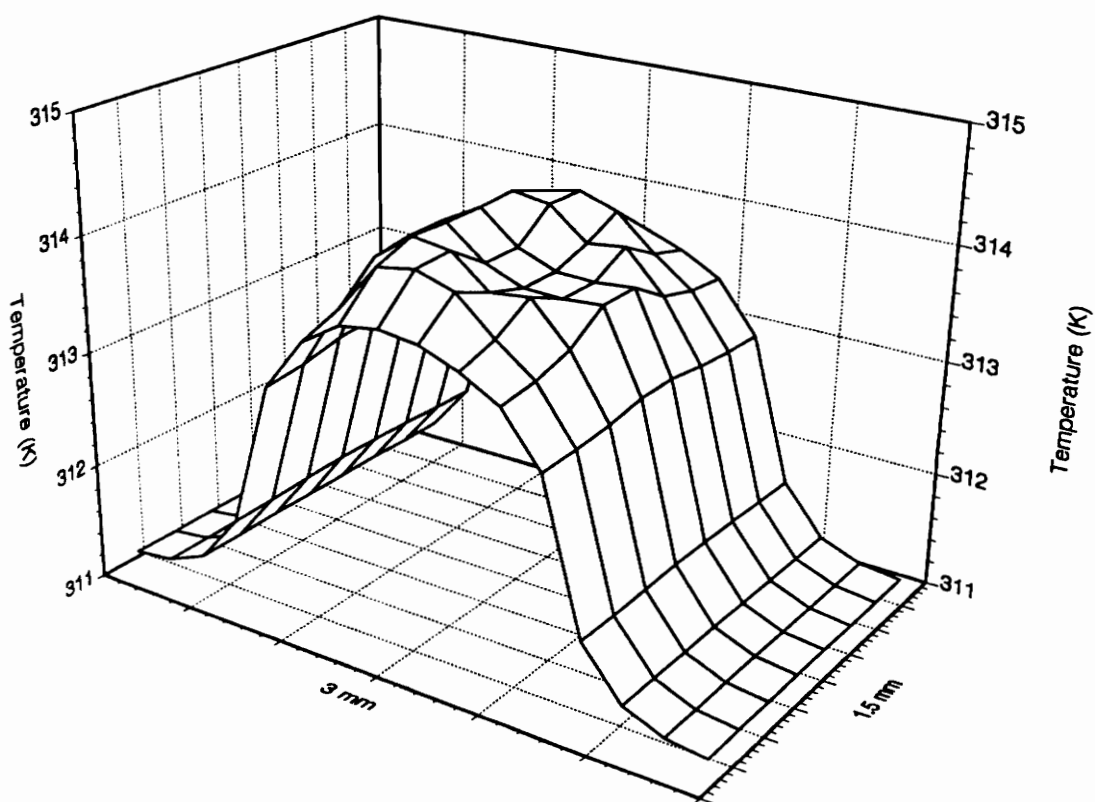


Fig. 27 **Equilibrium Two-Dimensional Temperature Distribution in the Active Thermistor for a 10-mW Nonuniform Source Power Input whose Shape is as in Fig. 26 but whose Size has been Increased to Fill the Absorber Surface.**

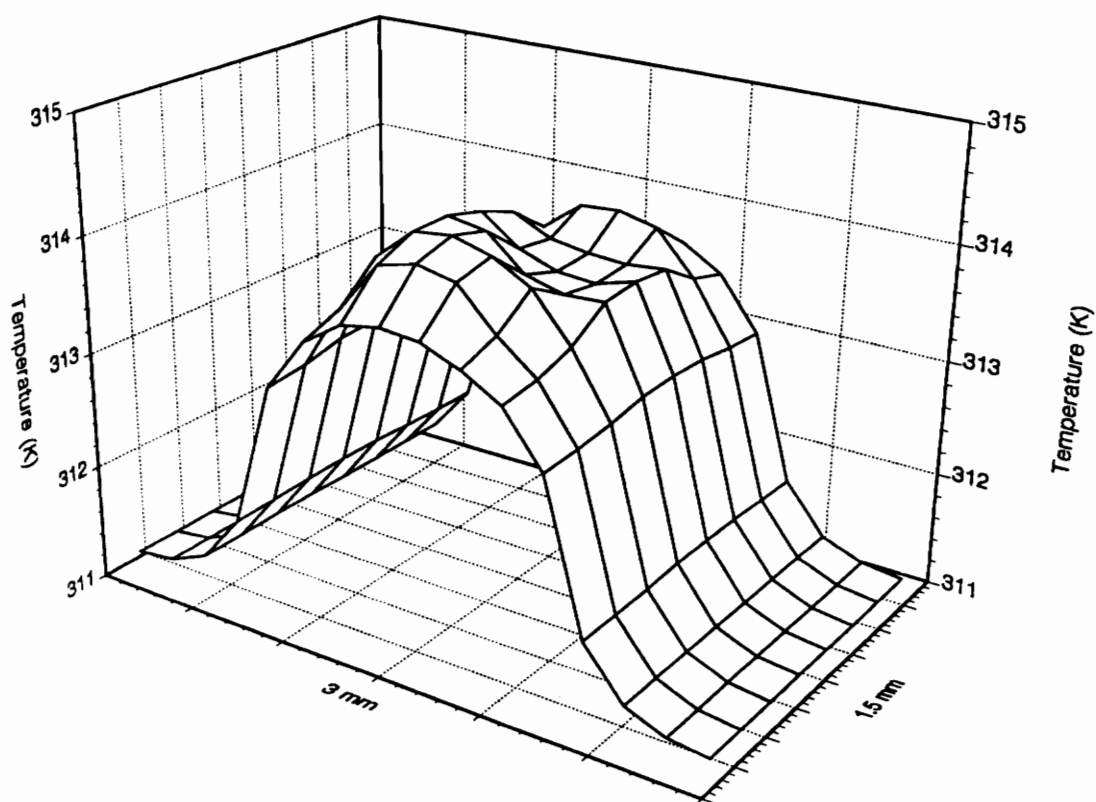


Fig. 28 **Equilibrium Two-Dimensional Temperature Distribution in the Active Thermistor for the-10 mW Nonuniform Source Power Input of Fig. 27 Rotated 45 deg.**

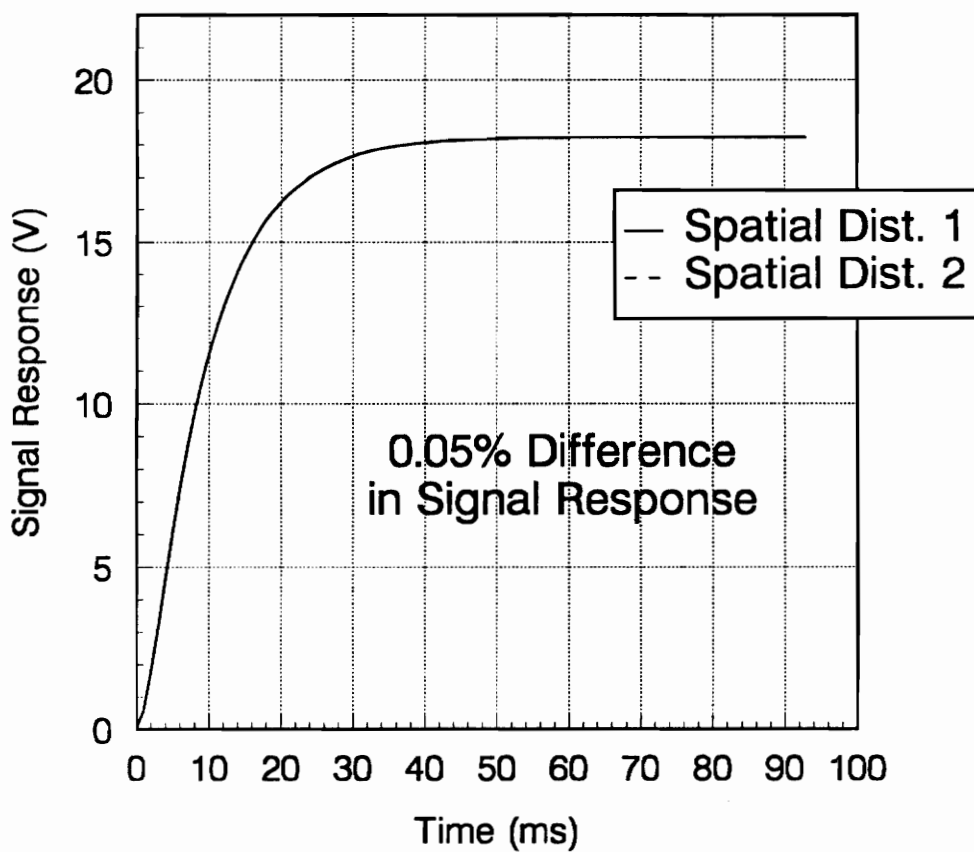


Fig. 29 Electronic Output as a Function of Time for the Radiative Heating Situations of Figs. 27 and 28.

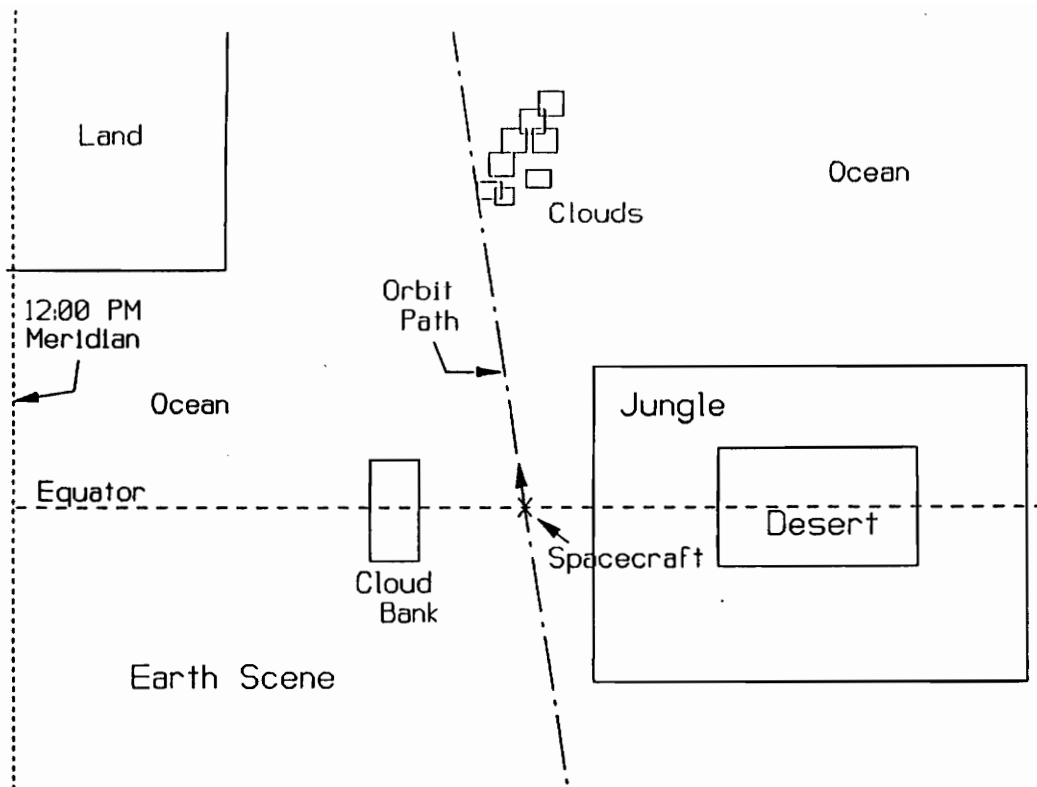


Fig. 30 Hypothetical Earth Scene Used to Generate a Numerical Earth Scan [34].

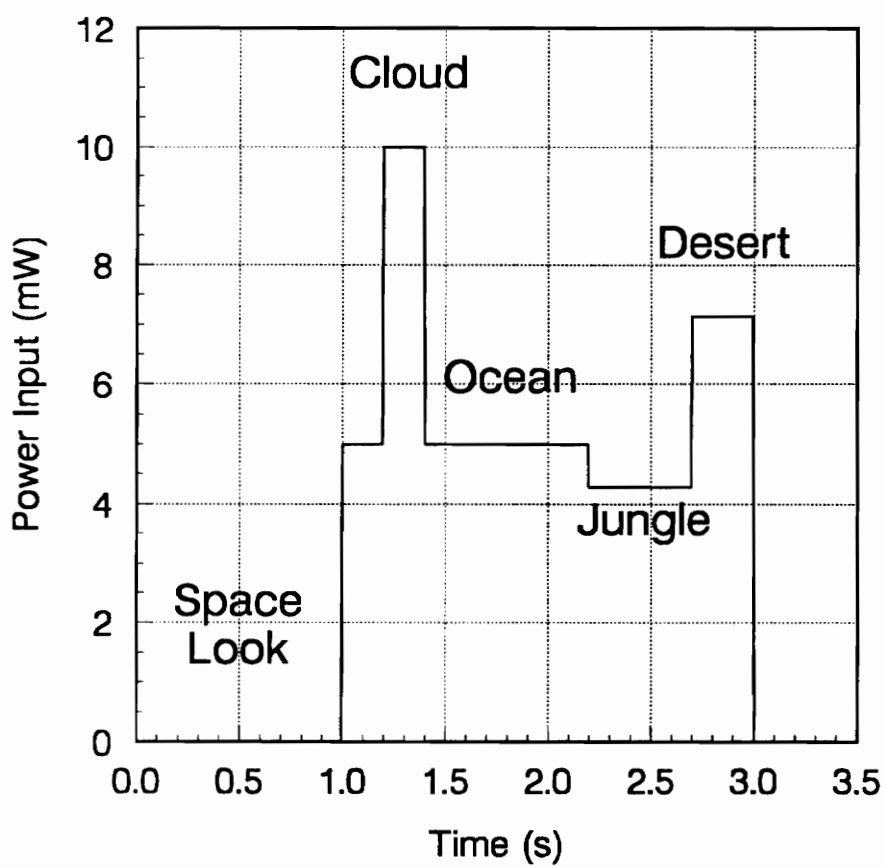


Fig. 31 **Power Input to the Active Flake Corresponding to a Numerical Earth Scan Simulation Based on Fig. 30.**

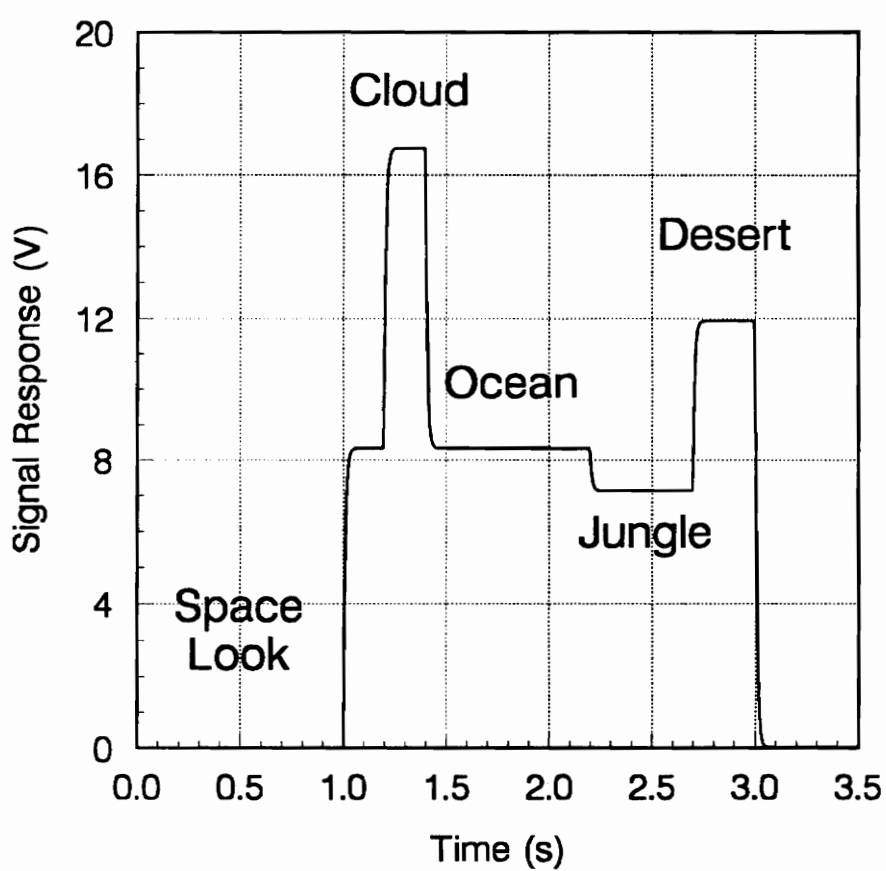


Fig. 32 **Electronic Output Corresponding to the Numerical Earth Scan Simulation of Fig. 31.**

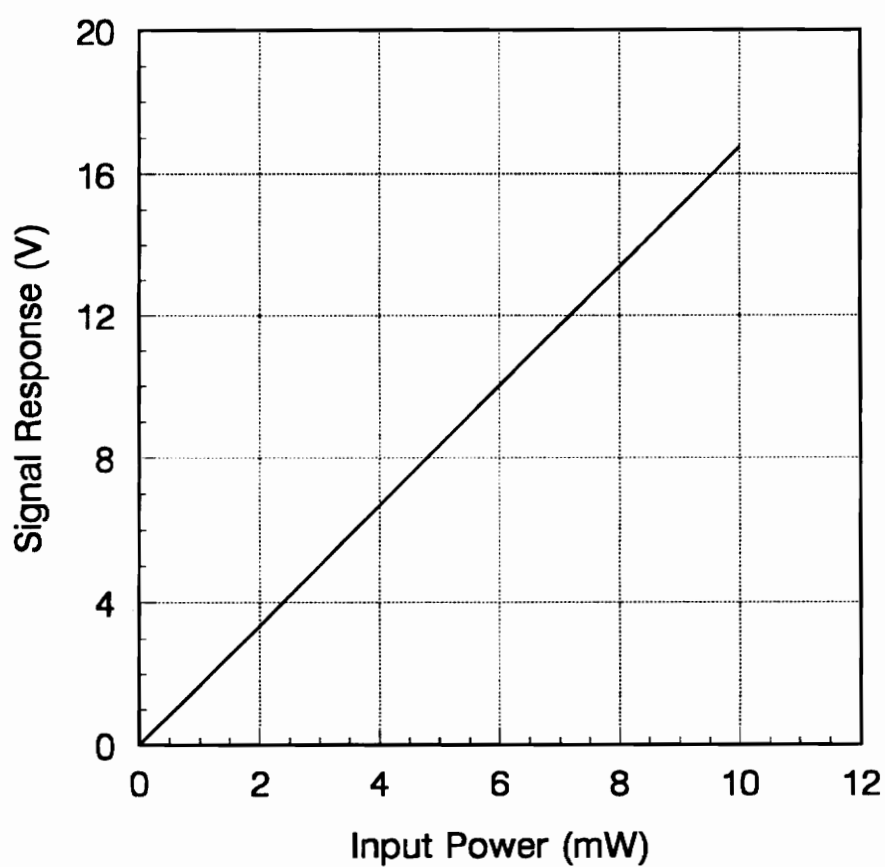


Fig. 33 **Equilibrium Electronic Output as a Function of the Power Input to the Detector for the Simulated Earth Scan of Fig. 31.**

References

1. Smith, G. L., Charlock, T. P., Crommelynck, D. A., Rutan, D., Gupta, S. K., and Rose, F. G., *Atmospheric Radiative Flux Divergence from Cloud and Earth Radiant Energy System*, **Proceedings of SPIE—The International Society for Optical Engineering**, Vol. 1299, 1990, pp 202-210.
2. Kann, D. M., Miller, A. J., and Yang, S., *Atmospheric Energetics and Earth Radiation Budget*, **Proceedings of SPIE—The International Society for Optical Engineering**, Vol. 1299, 1990, pp 40-49.
3. Duband, D., *Reflexions sur l'Utilisation des Longues Séries d'Observation Climatologiques dans le Cadre de l'Etude du Climat et de son Evolution*, **Houille Blanche**, Vol. 45, No. 6, 1990, pp 399-407.
4. Ramanathan, V., *Use of Earth Radiation Budget Measurements for Understanding Climate Changes*, **Proceedings of SPIE—The International Society for Optical Engineering**, Vol. 1299, 1990, pp 2-9.
5. Kandel, R., and Fouquart, Y., *Le Bilan Radiatif de la Terre*, **La Recherche**, Vol. 23, No. 241, March 1992, pp 312-324.
6. Cess, R. D., *General Circulation Model Intercomparisons for Understanding Climate*, **Proceedings of SPIE—The International Society for Optical Engineering**, Vol. 1299, 1990, pp 10-15.
7. Randall, D. A., *Atmospheric and Surface Cloud Radiative Forcing: Results from Climate Models*, **Proceedings of SPIE—The International Society for Optical Engineering**, Vol. 1299, 1990, pp 16-26.
8. Ramanathan, V., Cess, R. D., Harrisson, E. F., Minnis, P., Barkstrom, B. R., Ahmad, E., Hartmann, D., *Cloud Radiative Forcing and Climate: Results from the Earth Radiation Budget Experiment*, **Science**, Vol. 243, January 1989, pp 57-63.
9. Kyle, H. L., *Nimbus-7 Earth Radiation Budget Data Set and its Uses*, **Proceedings of SPIE—The International Society for Optical Engineering**, Vol. 1299, 1990, pp 27-39.

10. Barkstrom, B. R., *Earth Radiation Budget Measurements: pre-ERBE, ERBE, and CERES*, **Proceedings of SPIE—The International Society for Optical Engineering**, Vol. 1299, 1990, pp 52-60.
11. Siegel, R., Howell, J. R., **Radiation Heat Transfer**, 2nd Edition, Hemisphere Publishing Corporation, New York, 1981.
12. Darnell, W. L., Staylor, W. F., Gupta, S. K., Wilber, A. C., and Ritchey, N. A., *Surface Radiation Budget: Current Perspective*, **Proceedings of SPIE—The International Society for Optical Engineering**, Vol. 1299, 1990, pp 176-189.
13. Barkstrom, B. R., *The Earth Radiation Budget Experiment (ERBE)*, **Bulletins of the American Meteorological Society**, Vol. 65, No. 11, 1984, pp 1170-1185.
14. Kopia, L. P., and Lee III, R. B., *Earth Radiation Budget Experiment Scanner Instrument*, **Reviews of Geophysics**, Vol. 24, No. 2, May 1986, pp 400-406.
15. Fanney II, A. H., **Experimental Study of the LZEEBE Measurement System under Simulated Flight Conditions**, M. S. Thesis, Mechanical Engineering Department, Virginia Polytechnic Institute and State University, Blacksburg, VA (1975).
16. Rasnic, R. L., **A Thermal and Kinematic Model of a Thin-Wall Spherical Shell Satellite**, M. S. Thesis, Mechanical Engineering Department, Virginia Polytechnic Institute and State University, Blacksburg, VA (1975).
17. Passwaters III, J. O., **Detailed Thermal Analysis of a Thin-Shell, Spherical Radiometer in Earth Orbit**, M. S. Thesis, Mechanical Engineering Department, Virginia Polytechnic Institute and State University, Blacksburg, VA (1976).
18. Eskin, L. D., **Application of the Monte Carlo Method to the Transient Thermal Modeling of a Diffuse-Specular Radiometer Cavity**, M. S. Thesis, Mechanical Engineering Department, Virginia Polytechnic Institute and State University, Blacksburg, VA (1981).
19. Gardiner, B. D., **An Analytical Study of Dynamic Response and Nonequivalence of an Absolute Active Cavity Radiometer Operating at Cryogenic Temperatures**, M. S. Thesis, Mechanical Engineering Department, Virginia Polytechnic Institute and State University, Blacksburg, VA (1986).

20. Tira, N. E., **Dynamic Simulation of Solar Calibration of the Total, Earth-Viewing Channel of the Earth Radiation Budget Experiment (ERBE)**, M. S. Thesis, Mechanical Engineering Department, Virginia Polytechnic Institute and State University, Blacksburg, VA (1987).
21. Meekins, J. L., **Optical Analysis of ERBE Scanning Thermistor Bolometer Radiometer Using the Monte-Carlo Method**, M. S. Thesis, Mechanical Engineering Department, Virginia Polytechnic Institute and State University, Blacksburg, VA (1990).
22. Tira, N. E., **A Study of the Thermal and Optical Characteristics of Radiometric Channels for the Earth Radiation Budget Applications**, Ph. D. Dissertation, Mechanical Engineering Department, Virginia Polytechnic Institute and State University, Blacksburg, VA (1991).
23. Tira, Nour E., J. R. Mahan, Robert B. Lee, III, and R. J. Keynton, *Linear-Array Apertures for Inflight Dynamic Solar Calibration of Radiometric Channels for Earth Radiation Budget Applications*, **Applied Optics**, in press.
24. Lee, Robert B., III, M. Alan Gibson, Susan Thomas, J. Robert Mahan, Jeffrey L. Meekins, and N. E. Tira, *Earth Radiation Budget Experiment Scanner Radiometric Calibration Results*, **SPIE Vol. 1299, Long-Term Monitoring of the Earth's Radiation Budget**, April 17-18, 1990, Orlando, FL, pp. 80-91.
25. Tira, Nour E., J. R. Mahan, J. L. Meekins, R. B. Lee, III, and R. J. Keynton, *Optical Characterization of Scanning Thermistor Bolometer Radiometers Using Monte-Carlo Ray Trace Techniques*, **International Radiation Symposium**, Tallinn, Estonia, August 3-8, 1992.
26. Carman, S., **CERES Preliminary Design Review**, TRW Space & Technology, Los Angeles, CA, June 23-25, 1992.
27. Manolo, N., Smith, G. L., and Barkstrom, B. R., *Transfer Function Considerations for the CERES Scanning Radiometer*, **Proceedings of SPIE—The International Society for Optical Engineering**, Vol. 1521, 1991, pp 106-116.
28. Patankar, S. V., **Numerical Heat Transfer and Fluid Flow**, Hemisphere Publishing Corporation, New York, 1980.
29. Anon., Barnes Engineering Company, **ERBE Scanner Electronic Analysis**, May 23, 1980.
30. MicroSim Technical Support, **Personal Communications**, November, 1992.

31. Barnes Engineering Company, *Schematic of Electrical Preamplifier & Hi/Low Voltage Filter and Resistor Values*, **Documents Received from L. P. Kopia, NASA\Langley Research Center**, November 24, 1992.
32. Anon., MicroSim, **Reference Manual & User's Guide for PSpice**.
33. Kopia, L. P., *Thermophysical Properties of Flake Materials*, **Personal Communication**, August 14, 1992.
34. Anon., TRW Applied Technology Division, **End-to-End System Performance Analysis for Clouds and the Earth's Radiant Energy System (CERES)**, May 22, 1992.

Appendix A. Computer Program Listing

DYNASCAN


```
c steadytp:logical variables used in the convergence checks.
ccccccccccccccccccccccccccccccccccccccccccccccccccccccccccccccccccccc

implicit none

real*8 tp,ap,ap0,aw,ae,as,an,af,ab,bc,bp,tp0,tb,ti,te
real*8 delx,dely,delz,tau,deltau,length,width,thick,u,vv,tauadd
real*8 irx,irz,hache,conv,conv2,z,thertp,th2dtp
real*8 tcond,cond,tro,ro,tcp,cp,h,alpha,sigma,teleloss,relax
real*8 source,curden,resist,temp(20,20),ztemp
real*8 timmax,selfhea
real*4 onofx,onofy,onofz
integer i,j,k,t,nbiter,nnodth,cntstp,cout,cntout(10),noutpu
integer nbxint1,nbxint2,nbzint1,nbzint2,nbzint3,nbzint4,nbzint5
integer nbzint6,nbzint7,nbzint8
integer choice,repons,nbseha
integer nxmax,nymax,nzmax,nimax,njmax,nkmax,ntmax
integer nbdelx,nbdely,nbdelz,nbxint,nbzint,nz
logical goodtp,steady
parameter(nimax=20,njmax=10,nkmax=15,ntmax=5,nz=7)
dimension delz(nkmax),nbdelz(nz),thick(nz),irz(nkmax),irx(nimax)
dimension z(nkmax),source(nimax,nkmax)
dimension onofx(nimax,nkmax),onofy(njmax),onofz(nimax,nkmax)
dimension tcond(nkmax),tro(nkmax),tcp(nkmax),h(nimax,njmax)
dimension cond(nimax,nkmax),ro(nimax,nkmax),cp(nimax,nkmax)
dimension tp(nimax,njmax,nkmax,ntmax),tp0(nimax,njmax,nkmax,ntmax)

c
c prepare the output files
c file 3: 3-d temperature distribution when steady state is reached
c file 4: 1-d temperature distribution at each time step
c file 8: 2-d temp. Distr. In the thermistor at each time step
c file 9: average temperature of the thermistor at each time step
c
      write(03,603)
      write(04,604)
      write(08,607)
      write(09,608)
603   format(1x,'current density in the thermistor flake.'//)
604   Format(1x,'1-d (z-dir) temp. Distr. At each time step'//)
607   format(1x,'2-d temp. Distr. In the thermistor at each time step'//)
608   format(1x,'average temperature of the thermistor at each time step
&'//)
      tauadd=0.0D0

c
c menu
c
97    write(06,700)
      read(05,*)choice

c
c read input file
c
      read(01,*)
      read(01,*)

c
c convergence creteria
c
      read(01,*)conv
      read(01,*)conv2

c
c read alpha and sigma
c
```

```

        read(01,*)alpha
        read(01,*)sigma
c
c read the geometry of the thermistor flake
c
        read(01,*)length
        read(01,*)width
        read(01,*)
        do 5 k=1,nz
            read(01,*)thick(k)
5        continue
c
c read the thermal conductivities of each layer
c
        read(01,*)
        do 6 k=1,nz
            read(01,*)tcond(k)
6        continue
c
c read the volumetric mass of each layer
c
        read(01,*)
        do 7 k=1,nz
            read(01,*)tro(k)
7        continue
c
c read the specific heat of each layer
c
        read(01,*)
        do 8 k=1,nz
            read(01,*)tcp(k)
8        continue
c
c read the number of division in each direction
c
        read(01,*)nbdelx1
        read(01,*)nbdelx2
        nbdelx=2*nbdelx1+nbdelx2
        read(01,*)nbdely
        read(01,*)
        do 10 k=1,nz
            read(01,*)nbdelz(k)
10       continue
c
c set x and z interface numbering
c
        nbxint1=nbdelx1+1
        nbxint2=nbxint1+nbdelx2
*       write(06,*)'nbx 1 & 2',nbxint1,nbxint2
        nbzint1=2
        nbzint2=nbdelz(1)+nbzint1
        nbzint3=nbdelz(2)+nbzint2
        nbzint4=nbdelz(3)+nbzint3
        nbzint5=nbdelz(4)+nbzint4
        nbzint6=nbdelz(5)+nbzint5
        nbzint7=nbdelz(6)+nbzint6
        nbzint8=nbdelz(7)-1+nbzint7
c
c compute the steps in the x, y, and z-directions
c
        delx=length/dble(nbdelx)
        dely=width/dble(nbdely)

```

```

c absorber layer

      do 81 k=1,nbzint2-1
        delz(k)=thick(1)/dble(nbdelz(1))
81      continue

c bond/sealant layer

      do 82 k=nbzint2,nbzint3-1
        delz(k)=thick(2)/dble(nbdelz(2))
82      continue

c gold pad layer

      do 83 k=nbzint3,nbzint4-1
        delz(k)=thick(3)/dble(nbdelz(3))
83      continue

c thermistor layer

      do 84 k=nbzint4,nbzint5-1
        delz(k)=thick(4)/dble(nbdelz(4))
84      continue

c bonding layer

      do 85 k=nbzint5,nbzint6-1
        delz(k)=thick(5)/dble(nbdelz(5))
85      continue

c thermal impedance

      do 86 k=nbzint6,nbzint7-1
        delz(k)=thick(6)/dble(nbdelz(6))
86      continue

c second bonding layer

      do 87 k=nbzint7,nbzint8-1
        delz(k)=thick(7)*(2.D0/(2.D0*dble(nbdelz(7))-1.D0))
87      continue
      delz(nbzint8)=thick(7)*(1.D0/(2.D0*dble(nbdelz(7))-1.D0))
c
c compute the maximum c.v. index number for each direction
c
      nxmax=nbdelx+2
      nymax=nbdely+2
      nzmax=1
      do 12 k=1,nz
        nzmax=nzmax+nbdelz(k)
12      continue
c
c compute the cumulative thickness in the z direction
c
      z(1)=0.D0
      z(2)=0.5D0*delz(2)*1.0D6
      do 88 k=3,nzmax-1
        z(k)=z(k-1)+(0.5D0*(delz(k-1)+delz(k)))*1.0D6
88      continue
      z(nzmax)=z(nzmax-1)+(0.5D0*delz(k-1)+delz(k))*1.0D6
c
c read the time incrementation delta t

```

```

c      read(01,*)deltau
c read the relaxation factor
      write(06,*)'please specify the relaxation factor (over>1,under<1)'
      read(05,*)relax
c
c read initial guess for temperature
c
      read(01,*)ti
c
c read the boundary conditions:
c read heat sink temperature
c
      read(01,*)tb
c
c read the temperature of the surrounding
c
      te=tb
c
c read/set up the incoming radiative flux spatial distribution
c
      do 58 i=1,nxmax
      do 58 j=1,nymax
        h(i,j)=0.D0
58      continue
      if (choice.Ne.1) Then
        do 65 i=nbxint1+1,nbxint2
        do 65 j=2,nymax-1
          read(21,*)h(i,j)
65      continue
      rewind 21
444      write(06,601)nbxint1+1,nbxint1+2,nbxint1+3,nbxint1+4,nbxint1+5
&      ,nbxint1+6,nbxint1+7,nbxint2
      do 66 j=2,nymax-1
        write(06,600)j,h(nbxint1+1,j),h(nbxint1+2,j),h(nbxint1+3,j),
&      h(nbxint1+4,j),h(nbxint1+5,j),h(nbxint1+6,j),
&      h(nbxint1+7,j),h(nbxint2,j)

66      continue
600      format(i3,8f9.1)
601      Format(3x,8i9)
      write(06,*)'modify the distribution of the heat flux? (0/1)'
      Read(05,*)repons
      if (repons.Eq.1) Then
        write(06,*)'specify incident radiative heat flux (w/m2)'
        read(05,*)hache
        write(06,*)'specify the number of surface elmts impided'
        read(05,*)nbseha
        do 67 i=1,nxmax
        do 67 j=1,nymax
          h(i,j)=0.D0
67      continue
        if (nbseha.Eq.0) Then
          do 59 i=nbxint1+1,nbxint2
          do 59 j=2,nymax-1
            h(i,j)=hache
59      continue
        else
          write(06,*)'enter i,j for each surface element'
          do 68 k=1,nbseha
            read(05,*)i,j

```

```

        h(i,j)=hache
68      continue
        do 69 i=nbxint1+1,nbxint2
        do 69 j=2,nymax-1
            write(21,*)h(i,j)
69      continue
        end if
        rewind 21
        go to 444
    end if
end if
rewind 21
c
c read the time during which the flake is exposed to the heat flux
c
    write(06,*)'please specify the amount of time during which the fla
&ke is exposed to the heat flux, in seconds.'
    Read(05,*)timmax
c
c read the energy loss coefficient (through the telescope)
c
    read(01,*)teleloss
c
c read the output times
c
    read(01,*)noutpu
    do 335 i=1,noutpu
        read(01,*)cntout(i)
335    continue
c
c read selfheating value (w)
c
    read(01,*)selfhea
c
c return to top of input file
c
    rewind 1
c
c compute the thermal conductivities for all the control volumes
c
    do 70 i=1,nxmax
c absorber layer
        do 71 k=1,nbzint2-1
            cond(i,k)=tcond(1)
            ro(i,k)=tro(1)
            cp(i,k)=tcp(1)
71    continue
c bond/sealant layer
        do 72 k=nbzint2,nbzint3-1
            cond(i,k)=tcond(2)
            ro(i,k)=tro(2)
            cp(i,k)=tcp(2)
72    continue
c gold pad layer
        do 73 k=nbzint3,nbzint4-1
            cond(i,k)=tcond(3)

```

```

        ro(i,k)=tro(3)
        cp(i,k)=tcp(3)
73      continue

c thermistor layer

        do 74 k=nbzint4,nbzint5-1
            cond(i,k)=tcond(4)
            ro(i,k)=tro(4)
            cp(i,k)=tcp(4)
74      continue

c bonding layer

        do 75 k=nbzint5,nbzint6-1
            cond(i,k)=tcond(5)
            ro(i,k)=tro(5)
            cp(i,k)=tcp(5)
75      continue

c thermal impedance

        do 76 k=nbzint6,nbzint7-1
            cond(i,k)=tcond(6)
            ro(i,k)=tro(6)
            cp(i,k)=tcp(6)
76      continue

c second bonding layer

        do 77 k=nbzint7,nbzint8
            cond(i,k)=tcond(7)
            ro(i,k)=tro(7)
            cp(i,k)=tcp(7)
77      continue
70      continue

c bond/sealant layer between the gold pads

        do 78 i=nbxint1+1,nbzint2
            do 78 k=nbzint3,nbzint4-1
                cond(i,k)=tcond(2)
                ro(i,k)=tro(2)
                cp(i,k)=tcp(2)
78      continue
c
c set up boundary volume elements where (dt/dn)=0
c
        do 15 i=1,nxmax
            do 15 k=1,nzmax
                onofx(i,k)=1.0
                Onofz(i,k)=1.0
15      Continue
            do 16 j=1,nymax
                onofy(j)=1.0
16      Continue
            onofy(1)=0.0
            Onofy(nymax)=0.0
            Do 17 k=1,nzmax
                onofx(1,k)=0.0
                Onofx(nxmax,k)=0.0
                Onofz(1,k)=0.0

```

```

        Onofz(nxmax,k)=0.0
17  Continue
    do 20 i=2,nbxint1
    do 20 k=1,nbzint2-1
        onofx(i,k)=0.0
        Onofz(i,k)=0.0
20  Continue
    do 21 i=nbxint1+1,nbxint2
        onofx(i,1)=0.0
        Onofz(i,1)=0.0
21  Continue
    do 22 i=nbxint2+1,nxmax-1
    do 22 k=1,nbzint2-1
        onofx(i,k)=0.0
        Onofz(i,k)=0.0
22  Continue
c
c set interface resistances between v.E. Of different phys. Properties
c
    do 40 i=1,nxmax
        irx(i)=0.D0
40  continue
    do 50 k=1,nzmax
        irz(k)=0.D0
50  continue
    irx(nbxint1)=0.D0
    irx(nbxint2)=0.D0
    irz(nbzint1)=0.D0
    irz(nbzint2)=0.D0
    irz(nbzint3)=0.D0
    irz(nbzint4)=0.D0
    irz(nbzint5)=0.D0
    irz(nbzint6)=0.D0
    irz(nbzint7)=0.D0
c
c start at time = 0
c
    tau=0.D0
    t=1
c
c initialization of all temperatures t time = 0
c
    do 300 k=2,nbzint2-1
    do 300 i=nbxint1+1,nbxint2
    do 300 j=2,nymax-1
        read(02,*)tp(i,j,k,t)
300  continue
    do 305 k=nbzint2,nzmax
    do 305 i=2,nxmax-1
    do 305 j=2,nymax-1
        read(02,*)tp(i,j,k,t)
305  continue
    rewind 2
c
c set heat sink boundary
c
    k=nzmax
    do 101 i=1,nxmax
    do 101 j=1,nymax
        tp(i,j,k,t)=tb
101  continue
c

```

```

c initialization of all temperatures for first time iteration
c
    t=2
    tau=deltau
    tauadd=tauadd + deltau
    do 102 i=1,nxmax
    do 102 j=1,nymax
        tp(i,j,nxmax,t)=tb
    do 102 k=1,nxmax-1
        tp(i,j,k,t)=ti
102  continue
    cntstp=1
    cout=1
    go to 96

c
c increment the time
c
98  tau=tau+deltau
    tauadd=tauadd + deltau
    cntstp=cntstp+1

c
c initialization of all temperatures at time t
c
    t=2
    do 103 i=1,nxmax
    do 103 j=1,nymax
    do 103 k=1,nxmax
        tp(i,j,k,t-1)=tp(i,j,k,t)
103  continue
c
c reset the iteration counter and the convergence flag
c
96  nbiter=0
c
c compute the internal heat generation (source) terms
c
    do 60 i=1,nxmax
    do 60 k=1,nxmax
        source(i,k)=0.D0
60  continue
    do 61 i=nbxint1+1,nbxint2
    do 61 k=nbzint4,nbzint5-1
        source(i,k)=selfhea/(12.0D-6*1.53D-3*1.53D-3)
61  continue
c
c visit of each point, with computation of the ap's of the neighbors
c
99  nbiter=nbiter+1
c
c memorize the temperatures at each grid point
c
    do 110 i=1,nxmax
    do 110 j=1,nymax
    do 110 k=1,nxmax
        tp0(i,j,k,t)=tp(i,j,k,t)
110  continue
    goodtp=.True.

c
c compute the temperature distribution in the thermistor flake
c start with the absorber which receives the radiation
c
    k=2

```



```

do 115 i=nbxint1+1,nbxint2
do 115 j=2,nymax-1
    bp=(4.D0*alpha*sigma*tp(i,j,k,t)*tp(i,j,k,t)*tp(i,j,k,t))/
&    delz(k)
    bc=alpha*(h(i,j)*teleloss+sigma*(te*te*te*te*(1.D0-teleloss)+
&    3.D0*tp(i,j,k,t)*tp(i,j,k,t)*tp(i,j,k,t)*tp(i,j,k,t)))/delz(k)
    ae=onofx(i+1,k)/(delx*(delx/(2.D0*cond(i,k))+irx(i)+delx/(2.D0
&    *cond(i+1,k))))
    aw=onofx(i-1,k)/(delx*(delx/(2.D0*cond(i,k))+irx(i-1)+delx/(
&    2.D0*cond(i-1,k))))
    af=onofy(j+1)/(dely*dely/cond(i,k))
    ab=onofy(j-1)/(dely*dely/cond(i,k))
    as=onofz(i,k+1)/(delz(k)*(delz(k)/(2.D0*cond(i,k))+irz(k)+
&    delz(k+1)/(2.D0*cond(i,k+1))))
    an=onofz(i,k-1)/(delz(k)*(delz(k)/(2.D0*cond(i,k))+irz(k-1)+
&    delz(k-1)/(2.D0*cond(i,k-1))))
    ap0=ro(i,k)*cp(i,k)/deltau
    ap=ap0+ae+aw+af+ab+as+an+bp
    tp(i,j,k,t)=relax*(ap0*tp(i,j,k,t-1)+ae*tp(i+1,j,k,t)
&    +aw*tp(i-1,j,k,t)+af*tp(i,j+1,k,t)+ab*tp(i,j-1,k,t)
&    +as*tp(i,j,k+1,t)+an*tp(i,j,k-1,t)+bc+source(i,k))
&    /ap+(1.D0-relax)*tp0(i,j,k,t)
    if (dabs(tp(i,j,k,t)-tp0(i,j,k,t)).Gt.Conv) goodtp=.False.
115 Continue
c
c compute the temperatures in the absorber
c
do 120 k=3,nbzint2-1
do 120 i=nbxint1+1,nbxint2
do 120 j=2,nymax-1
    ae=onofx(i+1,k)/(delx*(delx/(2.D0*cond(i,k))+irx(i)+delx/(2.D0
&    *cond(i+1,k))))
    aw=onofx(i-1,k)/(delx*(delx/(2.D0*cond(i,k))+irx(i-1)+delx/(
&    2.D0*cond(i-1,k))))
    af=onofy(j+1)/(dely*dely/cond(i,k))
    ab=onofy(j-1)/(dely*dely/cond(i,k))
    as=onofz(i,k+1)/(delz(k)*(delz(k)/(2.D0*cond(i,k))+irz(k)+
&    delz(k+1)/(2.D0*cond(i,k+1))))
    an=onofz(i,k-1)/(delz(k)*(delz(k)/(2.D0*cond(i,k))+irz(k-1)+
&    delz(k-1)/(2.D0*cond(i,k-1))))
    ap0=ro(i,k)*cp(i,k)/deltau
    ap=ap0+ae+aw+af+ab+as+an
    tp(i,j,k,t)=relax*(ap0*tp(i,j,k,t-1)+ae*tp(i+1,j,k,t)
&    +aw*tp(i-1,j,k,t)+af*tp(i,j+1,k,t)+ab*tp(i,j-1,k,t)
&    +as*tp(i,j,k+1,t)+an*tp(i,j,k-1,t)+source(i,k))
&    /ap+(1.D0-relax)*tp0(i,j,k,t)
    if (dabs(tp(i,j,k,t)-tp0(i,j,k,t)).Gt.Conv) goodtp=.False.
120 Continue
c
c compute the temperatures in the following control volumes
c
do 125 k=nbzint2,nzmax-1
do 125 i=2,nxmax-1
do 125 j=2,nymax-1
    ae=onofx(i+1,k)/(delx*(delx/(2.D0*cond(i,k))+irx(i)+delx/(2.D0
&    *cond(i+1,k))))
    aw=onofx(i-1,k)/(delx*(delx/(2.D0*cond(i,k))+irx(i-1)+delx/(
&    2.D0*cond(i-1,k))))
    af=onofy(j+1)/(dely*dely/cond(i,k))
    ab=onofy(j-1)/(dely*dely/cond(i,k))
    as=onofz(i,k+1)/(delz(k)*(delz(k)/(2.D0*cond(i,k))+irz(k)+
&    delz(k+1)/(2.D0*cond(i,k+1))))

```

```

        an=onofz(i,k-1)/(delz(k)*(delz(k)/(2.D0*cond(i,k))+irz(k-1)+
&      delz(k-1)/(2.D0*cond(i,k-1))))
        ap0=ro(i,k)*cp(i,k)/deltau
        ap=ap0+ae+aw+af+ab+as+an
        tp(i,j,k,t)=relax*(ap0*tp(i,j,k,t-1)+ae*tp(i+1,j,k,t)
&      +aw*tp(i-1,j,k,t)+af*tp(i,j+1,k,t)+ab*tp(i,j-1,k,t)
&      +as*tp(i,j,k+1,t)+an*tp(i,j,k-1,t)+source(i,k))
&      /ap+(1.D0-relax)*tp0(i,j,k,t)
        if (dabs(tp(i,j,k,t)-tp0(i,j,k,t)).Gt.Conv) goodtp=.False.
125  Continue
c
c test for convergence of the temperature for the current time step
c
        if (nbiter.Lt.5000.And..Not.Goodtp) go to 99
        write(06,560)cntstp,nbiter
c
c store the 2-d temp. Distribution of thermistor for potential comput.
c
        do 93 i=nbxint1,nbxint2+1
        do 93 j=2,nymax-1
            temp(i-nbdelx1,j)=2.D0*tp(i,j,7,t)*tp(i,j,8,t)/
&          (tp(i,j,7,t)+tp(i,j,8,t))
93  continue
c
c compute the average resistance of the active flake
c
        call heagen(temp,curden,resist)
c
c
c compute selfheating to be used in next time step using correlations
c obtained from the electronical analysis
c
        if (choice.Ne.1) Then
            selfhea = -8.8038126D-8*resist + 0.0636188D0
            write(12,581)selfhea
        end if
581  format(f15.6)
c
c output of the average thermistor resistance at each time step
c
        if (choice.Ne.1) Then
            write(11,580)tauadd,(0.14D0*resist+101.D3)
            write(10,580)tauadd,resist
        end if
580  format(' + ( ',f15.6,' , ',F15.6,' ) ')
c
c the temp. Distributions are printed at particular time steps only
c
        if (cntstp.Eq.Cntout(cout).And.Choice.Ne.1) Then
            cout=cout + 1
c
c output of temperature distribution in the z-direction
c
        write(04,510)tau*1.D3
        do 200 k=2,nzmax
            ztemp=0.D0
            do 201 i=nbxint1+1,nbxint2
            do 201 j=2,nymax-1
                ztemp=ztemp + tp(i,j,k,t)
201  continue
            nnodth=(nbxint2-nbxint1)*(nymax-2)
            ztemp=ztemp/nnodth

```

```

write(04,540)z(k),ztemp
200 continue
c
c output of thermistor temperature
c
      write(08,510)tau*1.D3
      write(08,555)0.0D0,dely*0.5D3,dely*1.5D3,dely*2.5D3,dely*3.5D3,dely*4.5D3,dely*5.5D3,dely*6.5D3,dely*7.5D3
      do 210 i=2,nxmax-1
          uu=(dble(i)-1.5D0)*delx*1.D3
          write(08,555)uu,tp(i,2,7,t),tp(i,3,7,t),tp(i,4,7,t),tp(i,5,7,t)&
&,tp(i,6,7,t),tp(i,7,7,t),tp(i,8,7,t),tp(i,9,7,t)
210   continue
      end if
c
c output of average thermistor temperature (at each time step)
c
      if (choice.Ne.1) Then
          thertp=0.D0
          do 215 k=nbzint4,nbzint5-1
              do 215 i=nbxint1+1,nbxint2
                  do 215 j=2,nymax-1
                      thertp=thertp+tp(i,j,k,t)
215   continue
              nnodth=(nbzint5-nbzint4)*(nbxint2-nbxint1)*(nymax-2)
              thertp=thertp/nnodth
              write(09,550)tau*1.D3,thertp
          end if
c
c test if the temperature in the flake reached steady state
c
          steady=.True.
          do 175 k=2,nbzint2-1
              do 175 i=nbxint1+1,nbxint2
                  do 175 j=2,nymax-1
                      if (dabs(tp(i,j,k,t)-tp(i,j,k,t-1)).Gt.Conv2) steady=.False.
175   Continue
              do 176 k=nbzint2,nzmax
                  do 176 i=2,nxmax-1
                      do 176 j=2,nymax-1
                          if (dabs(tp(i,j,k,t)-tp(i,j,k,t-1)).Gt.Conv2) steady=.False.
176   Continue
                      if (choice.Eq.1.Or.Choice.Eq.2) Then
                          if (cntstp.Lt.500.And..Not.Steady) go to 98
                      else if (choice.Eq.3) Then
                          if (tau.Lt.Timmax) go to 98
                      end if
c
ccccccccccccccccccccccccccccccccccccccccccccccccccccccccccccccccc
c                                                                    c
c                final output after steady state is reached        c
c                                                                    c
ccccccccccccccccccccccccccccccccccccccccccccccccccccccccccccccccc
c
c final output of the average resistance in the active and reference flakes

      if (choice.Eq.1) Then
          write(11,580)0.00000,0.14D0*resist + 101.D3
          write(10,580)0.00000,Resist
          tauadd=0.000D0
          end if
c
```

```

c final output of temperature distribution in the z-direction
c
    write(04,510)tau*1.D3
    do 202 k=2,nzmax
        ztemp=0.D0
        do 203 i=nbxint1+1,nbxint2
            do 203 j=2,nymax-1
                ztemp=ztemp + tp(i,j,k,t)
203      continue
        nnodth=(nbxint2-nbxint1)*(nymax-2)
        ztemp=ztemp/nnodth
        write(04,540)z(k),ztemp
202    continue
c
c final output of 2-d temperature distribution of thermistor in table format
c
    write(08,510)tau*1.D3
    write(08,555)0.0D0,dely*0.5D3,dely*1.5D3,dely*2.5D3,dely*3.5D3,dely*4.5D3,dely*5.5D3,dely*6.5D3,dely*7.5D3
    do 204 i=2,nxmax-1
        uu=(dble(i)-1.5D0)*delx*1.D3
        write(08,555)uu,tp(i,2,7,t),tp(i,3,7,t),tp(i,4,7,t),tp(i,5,7,t)
        &tp(i,6,7,t),tp(i,7,7,t),tp(i,8,7,t),tp(i,9,7,t)
204    continue
c
c final output of thermistor temperature for contour plot
c
    do 205 i=2,nxmax-1
        do 205 j=2,nymax-1
            uu=(dble(i)-1.5D0)*delx*1.D3
            vv=(dble(j)-1.5D0)*dely*1.D3
            write(03,556)uu,vv,tp(i,j,7,t)
205    continue
c
c final output of average temperature of thermistor
c
    thertp=0.D0
    do 211 k=nbzint4,nbzint5-1
        do 211 i=nbxint1+1,nbxint2
            do 211 j=2,nymax-1
                thertp=thertp+tp(i,j,k,t)
211    continue
    nnodth=(nbzint5-nbzint4)*(nbxint2-nbxint1)*(nymax-2)
    thertp=thertp/nnodth
    write(09,550)tau*1.D3,thertp
c
c output of final temperature distribution in the 3 directions
c which is used as initial distribution if the program is executed
c again before quitting
c
    do 145 k=2,nbzint2-1
        do 145 i=nbxint1+1,nbxint2
            do 145 j=2,nymax-1
                write(02,570)tp(i,j,k,t)
145    continue
    do 150 k=nbzint2,nzmax
        do 150 i=2,nxmax-1
            do 150 j=2,nymax-1
                write(02,570)tp(i,j,k,t)
150    continue
    rewind 2
c

```

```

c end menu
c

write(06,*)'do you want to run it again? (0/1)'
Read(05,*)repons
if (repons.Eq.1) Then
  write(06,*)'reset time to zero?'
  Read(05,*)repons
  if (repons.Eq.1) Tauadd=0.0D0
  go to 97
end if
write(06,*)'initialize input file 1 before quitting? (0/1)'
Read(05,*)repons
if (repons.Eq.1) Then
  do 350 k=2,nbzint2-1
  do 350 i=nbxint1+1,nbxint2
  do 350 j=2,nymax-1
    write(02,*)311.15D0
350  continue
  do 355 k=nbzint2,nzmax
  do 355 i=2,nxmax-1
  do 355 j=2,nymax-1
    write(02,*)311.15D0
355  continue
  end if
  write(06,*)'do you really want to quit? (0/1)'
  Read(05,*)repons
  if (repons.Eq.0) Go to 97
c
c output format
c
500  format(1x,a3,i3,a3,i3,a3,i3,a15,f10.5)
510  Format(/1x,'after ',f4.1,' Milliseconds the temperature
&distribution is:')
530  format(1x,'the number of iteration performed is ',i5//)
540  format(1x,f8.3,F15.4)
550  Format(1x,2f10.5,F15.5)
555  Format(f4.2,8F9.4)
556  Format(2f6.3,F10.5)
560  Format(1x,'time step ',i4,' , ',i5,' iterations necessary')
570  format(1x,f15.5)
700  Format(65('=')//,16('='),' menu, please enter your choice. ',
&16('=')//,
&2X,'1. No radiative input; compute the temperature distribution.'/
&,2X,'2. Radiative input; compute the temperature distribution,'/,
&5x,'and the resistance until steady state is reached.','/,
&2X,'3. Radiative input, compute the temperature distribution,'/,
&5x,'and the resistance for a given duration'//,65('=')//)

end

```

```

*****
*
*                               Subroutine Heagen
*
* The following subroutine computes the average resistance of the ther-
* mistor layer based on the temperature distribution determined by the
* thermal model. It is based on a 2D fully implicit finite difference
* method.
*
*****
      subroutine heagen(tp,curden,resist)

c
c the variables are identical to the ones in the main program except for:
c ep, ep0: nodal electrical potential at time t, and t-Δt.
c e1, e2: electrical potential at across the thermistor layer.
c sigh, sigv: electrical conductivities.
c
      implicit none
      real*8 curint(20,20),resist,curden
      real*8 tp(20,20),ep,ep0,e1,e2,eguess
      real*8 ap,av,ah,tavh,tavv,sigh,sigv,sigh1,sigh2,sigv1,sigv2
      real*8 delx,dely,delz,length,width,uu
      real*8 conv,relax
      integer i,j,nbiter
      integer nxmax,nymax,nimax,njmax
      integer nbdelx,nbdely,nx,nz
      logical goodtp
      parameter(nimax=20,njmax=10,nx=6,nz=7)
      dimension av(nimax,njmax),ah(nimax,njmax),ap(nimax,njmax)
      dimension ep(nimax,njmax),ep0(nimax,njmax)

c
c set constants of the problem
c
      length=1.53D-3
      width=1.53D-3
      delz=12.0D-6

c
c convergence criteria
c
      conv=1.0D-9

c
c the number of division in each direction
c
      nbdelx=10
      nbdely=8

c
c compute the steps in the x, y, and z-directions
c
      delx=1.53D-3/dbl(nbdelx-2)
      dely=1.53D-3/dbl(nbdely)

c
c compute the maximum c.V. Index number for each direction
c
      nxmax=nbdelx
      nymax=nbdely+2

c
c the relaxation factor
c
      relax=1.7D0

```

```

c
c initial guess for temperature
c
      eguess=0.0D0
c
c boundary conditions: right potential e1 and left potential e2
c
      e1=0.0D0
      e2=75.0D0
c
c initial guess: initialization of all potentials ep @ time =delt, t=2
c
      do 60 i=1,nxmax
      do 60 j=1,nymax
          ep(i,j)=eguess
60      continue
      do 65 j=1,nymax
          ep(1,j)=e1
          ep(nxmax,j)=e2
65      continue
c
c ae and aw are respectively ah(i,j) and ah(i-1,j) for ep(i,j)
c as and an are respectively av(i,j) and av(i,j-1) for ep(i,j)
c
      do 100 i=1,nxmax
          av(i,1)=0.0D0
          av(i,nymax-1)=0.0D0
100      continue
      do 105 j=2,nymax-1
c
c for the first and last c.V. Sigma has to be computed a distance dx/4
c away from the 1st/last node; therefore the harmonic mean is applied
c twice for these nodes
c
          i=1
          sigh1=1.D0/(delz*width/length*250.D3*(1.D0-(tp(i,j)-298.15D0)
&          *0.035D0))
          sigh2=1.D0/(delz*width/length*250.D3*(1.D0-(tp(i+1,j)-298.15D0
&          )*0.035D0))
          sigh1=2.D0*sigh1*sigh2/(sigh1+sigh2)
          sigh=2.D0*sigh1*sigh2/(sigh1+sigh2)
          ah(i,j)=sigh*dely/(delx/2.D0)
          i=nxmax-1
          sigh1=1.D0/(delz*width/length*250.D3*(1.D0-(tp(i,j)-298.15D0)
&          *0.035D0))
          sigh2=1.D0/(delz*width/length*250.D3*(1.D0-(tp(i+1,j)-298.15D0
&          )*0.035D0))
          sigh1=2.D0*sigh1*sigh2/(sigh1+sigh2)
          sigh=2.D0*sigh1*sigh2/(sigh1+sigh2)
          ah(i,j)=sigh*dely/(delx/2.D0)
105      continue
c
c for interior nodes sigma is computed at the nodal points and the face
c values are computed using a harmonic mean
c first between horizontal nodes:
c
      do 110 i=2,nxmax-2
      do 110 j=2,nymax-1
          sigh1=1.D0/(delz*width/length*250.D3*(1.D0-(tp(i,j)-298.15D0)
&          *0.035D0))
          sigh2=1.D0/(delz*width/length*250.D3*(1.D0-(tp(i+1,j)-298.15D0
&          )*0.035D0))

```

```

        sigh=2.D0*sigh1*sigh2/(sigh1+sigh2)
        ah(i,j)=sigh*dely/delx
110    continue
c
c then between vertical nodes, with a special case for i=2 & i=nxmax-1
c
        do 112 j=2,nymax-2
            i=2
            sigv1=1.D0/(delz*width/length*250.D3*(1.D0-(tp(i,j)-298.15D0)
&            *0.035D0))
            sigv2=1.D0/(delz*width/length*250.D3*(1.D0-(tp(i,j+1)-298.15D0
&            )*0.035D0))
            sigv=2.D0*sigv1*sigv2/(sigv1+sigv2)
            av(i,j)=sigv*0.75D0*delx/dely
            i=nxmax-1
            sigv1=1.D0/(delz*width/length*250.D3*(1.D0-(tp(i,j)-298.15D0)
&            *0.035D0))
            sigv2=1.D0/(delz*width/length*250.D3*(1.D0-(tp(i,j+1)-298.15D0
&            )*0.035D0))
            sigv=2.D0*sigv1*sigv2/(sigv1+sigv2)
            av(i,j)=sigv*0.75D0*delx/dely
112    continue
        do 111 i=3,nxmax-2
        do 111 j=2,nymax-2
            sigv1=1.D0/(delz*width/length*250.D3*(1.D0-(tp(i,j)-298.15D0)
&            *0.035D0))
            sigv2=1.D0/(delz*width/length*250.D3*(1.D0-(tp(i,j+1)-298.15D0
&            )*0.035D0))
            sigv=2.D0*sigv1*sigv2/(sigv1+sigv2)
            av(i,j)=sigv*delx/dely
111    continue
c
c computation of ap's the coef. Of ep
c
        do 115 i=2,nxmax-1
        do 115 j=2,nymax-1
            ap(i,j)=ah(i-1,j) + ah(i,j) + av(i,j-1) + av(i,j)
115    continue
c
c reset the iteration counter and the convergence flag
c
        nbiter=0
c
c visit of each point, with computation of the ap's of the neighbors
c
99    nbiter=nbiter+1
c
c memorize the temperatures at each grid point
c
        do 200 i=1,nxmax
        do 200 j=1,nymax
            ep0(i,j)=ep(i,j)
200    continue
        goodtp=.True.

        Do 300 i=2,nxmax-1
        do 300 j=2,nymax-1
            ep(i,j)=relax*(ah(i,j)*ep(i+1,j)+ah(i-1,j)*ep(i-1,j)
&            +av(i,j)*ep(i,j+1)+av(i,j-1)*ep(i,j-1))/ap(i,j)
&            +(1.D0-relax)*ep0(i,j)
            if (dabs(ep(i,j)-ep0(i,j)).Gt.Conv) goodtp=.False.
300    Continue

```



```

C
C test for convergence of the temperature for the current time step
C
      if (nbiter.Lt.5000.And..Not.Goodtp) go to 99
*      write(06,*) 'nber iterations',nbiter
C
C computation of the current intensity in the x-direction
C computation of the overall average resistance
C
      curden=0.D0
      do 223 j=2,nymax-1
      do 222 i=2,nxmax-2
          sigh1=1.D0/(delz*width/length*250.D3*(1.D0-(tp(i,j)-298.15D0)
&          *0.035D0))
          sigh2=1.D0/(delz*width/length*250.D3*(1.D0-(tp(i+1,j)-298.15D0
&          )*0.035D0))
          sigh=2.D0*sigh1*sigh2/(sigh1+sigh2)
          curint(i,j)=(sigh*(ep(i+1,j)-ep(i,j)))/(delx/1.D0))*(delz*width)
          curden = curden + curint(i,j)
222      continue
223      continue
      curden = curden/((nxmax-3)*(nymax-2))
      resist=(e2 - e1)/curden
C
C output formats
C
530      format(1x,'the number of iteration performed is ',i5//)
540      format(1x,f8.3,F15.4)
550      Format(1x,2f10.5,F15.5)
555      Format(1x,f5.1,4F15.5)
556      Format(1x,f5.1,5F10.3)
568      Format(//1x,'average resistance of the thermistor',f15.2,' Ohm')
569      format(i3,3p,7f9.5)
571      Format(i3,7i9)
570      format(1x,f15.5)
      End

```

Vita

Martial P. Haeffelin was born in Boulogne-sur-Seine, France, on July 19, 1969, just a few hours before Neil Armstrong put the first human foot on the moon. In August, 1977, he moved to Stockholm, Sweden, and graduated from the *Lycée Saint-Louis* in July, 1987.

In September, 1987, Martial returned to France to start the engineering program at the *Université de Technologie de Compiègne*. During his undergraduate studies, Martial did a six-months training period as an assistant production engineer for PALL Europe, Ilfracombe, U.K., the world leader in fluid clarification.

In August, 1991, Martial started his graduate studies at Virginia Polytechnic Institute and State University as a graduate research assistant. In November, 1992, he received his *Diplôme d'Ingénieur* in Chemical Engineering and in February, 1993 he received his Master of Science in Mechanical Engineering.

Martial P. Haeffelin